Review

Experimental researches on quantum transport in semiconductor two-dimensional electron systems

By Shinji KAWAJI[*1,*2,†]

(Communicated by Jun KONDO, M.J.A.)

Abstract: The author reviews contribution of Gakushuin University group to the progress of the quantum transport in semiconductor two-dimensional electron systems (2DES) for forty years from the birth of the 2DES in middle of the 1960s till the finding of temperature dependent collapse of the quantized Hall resistance in the beginning of this century.

Keywords: two-dimensional electron systems, weak localization, transport properties in strong magnetic fields, quantum Hall effect

1. Introduction

Almost sixty years have passed since the transistor was born in an experimenral study of the electrical conduction on a germanium surface in Bell Telephone Laboratories.[1)] Since then, a lot of studies have been made on the electrical transport at the surface space charge layers in semiconductors.[2)]

Electrical transport phenomena associated with surfaces of solids have been well known in thin films of metals.[3)] Two scattering mechanisms of conduction electrons at the surface, namely the specular scattering and the diffuse scattering at the surface, are well known. It is known that the surface diffuse scattering, or the surface roughness scattering, plays a role in metallic thin films.

In semiconductor surface space charge layers, it has been observed that the mobility of conduction electrons and holes in both the surface inversion layers and the surface accumulation layers decreases with the increase in their concentrations. In 1955, Schrieffer explained this phenomenon by introducing the surface diffuse scattering or the surface roughness scattering into the theory of electron mobility in the semiconductor surface space charge layers.[4)] However, when the thickness of the surface space charge layer is thin enough compared with the wave length of electrons or holes in the surface space charge layer, the effect of the quantization of motion in the very thin layer may reduce the effect of the surface scattering.[5)–7)] In a thin surface space charge layer with a high electric field perpendicular to the surface (z-direction), the electron motion in z-direction is quantized like E_0, E_1 and so on as shown in Fig. 1(a). When the electrons are free in the motion parallel to the interface (xy plane), the energy of the electrons is given by

$$E = E_n + \frac{\hbar^2}{2m^*}(k_x^2 + k_y^2), \quad n = 0, 1, 2, - \qquad [1]$$

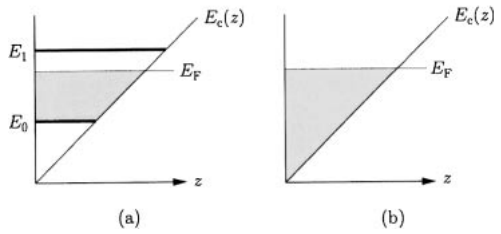

Fig. 1. In a triangular potential well near the surface of an inversion layer in a p-type semiconductor ($E_c(z)$: the bottom of the conduction band, E_F: the Fermi level), the kinetic motion of electrons perpendicular to the surface (z-direction) are quantized as E_0, E_1 and electrons fill the states with 2-dimensional freedom up to the E_F as shown in (a). When there is the surface diffuse scattering for electrons, the quantization of the electron motion disappears and the electrons fill the states with short mean free paths up to the Fermi level as shown in (b).

*1 Department of Physics, Gakushuin University, Tokyo, Japan.
*2 Recipients of the Japan Academy Prize in 2007.
† Correspondence should be addressed: S. Kawaji, Department of Physics, Gakushuin University, Mejiro, Toshima-ku, Tokyo 171-8588, Japan (e-mail: shinji.kawaji@gakushuin.ac.jp).

doi: 10.2183/pjab/84.199

where m^* is the electron effective mass, k_x and k_y are components of the wave vector for the motion in the plane parallel to the surface, and $E_n(n = 0, 1, --)$ is the electronic quantum level arising from confinement in the thin triangular-like quantum well. Each value of E_n is the bottom of a two-dimensional electron system (2DES), or a two-dimensional electron gas (2DEG), called a 2D-subband. The 2DES is characterized by its constant density of states given by

$$D_2 = \frac{g_s g_v m^*}{2\pi\hbar^2} \qquad [2]$$

where g_s and g_v are the spin and the valley degeneracy.

When a high magnetic field B is applied perpendicular to the 2-dimensional plane in a 2DES, the two dimensional free electron motion is converted to a set of quantized Landau levels with an energy splitting $\hbar\omega_c = \hbar eB/m^*$. The number of electrons in a magnetic quantum level is equal to the density of states, D_2, times the Landau level splitting, $\hbar\omega_c$ which is equal to eB/h in the case where $g_s = 1$ and $g_v = 1$.

In the International Conference on Physics of Semiconductors in Kyoto, 1966, Fowler *et al.*[8] reported magnetoconductance oscillations against the change in the gate voltage in a Corbino disk geometry of a Si-MOSFET where the peaks of the oscillation are uniformly spaced against the change in the gate voltage. This behavior shows clearly that the electron system in the Si-MOSFET is a 2DES. In the same conference, Kawaji and Kawaguchi[9] reported experimental results of electron mobility measurements in an n-type inversion layer on a p-type InAs as shown in Fig. 2. They compared the results with calculated values based on a two-dimensional version of the Conwell-Weisskopf[10] formula for ionized impurity scattering. The impurity scattering model in a 2DES explained well the exprimental result at 4.2 K.

In 1967, Stern and Howard[11] discussed theoretically basic electronic properties of 2DES in Si-MOSFETs and an n-channel inversion layer on a p-type InAs. On the latter, they calculated the electron mobility at absolute zero in an inversion layer on uncompensated p-type InAs with 6×10^{11} interface Coulomb scatterers per cm^2, the value estimated by Kawaji and Kawaguchi for their sample if all the centers are singly charged, and

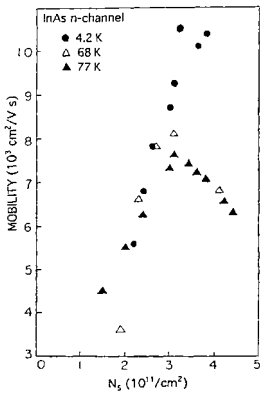

Fig. 2. In an n-type inversion layer of a p-type InAs surface, the electron mobility at 4.2 K increases with the increase in the surface concentration of electrons, N_s. This behavior can be explained by the decrease in the cross section of the scattering by charged impurities with the increase in the Fermi energy of the 2D electrons.[9]

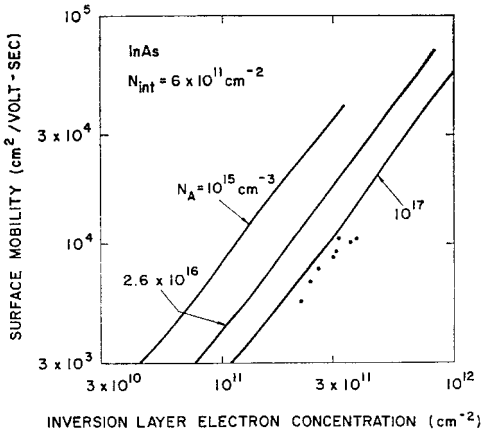

Fig. 3. Stern and Howard[11] calculated the low temperature mobility associated with screened Coulomb scattering by known charges in an inversion layer of a p-type InAs surface in the Born approximation. Their results are in good agreement with Kawaji and Kawaguchi's experimental results at 4.2 K[9] shown by dots in the figure.

for several values of bulk-acceptor concentration N_A. The results are shown in Fig. 3 together with the mobilities measured by Kawaji and Kawaguchi on a sample with 2.6×10^{16} net acceptors per cm^3. Over the experimental range, their calculated mobility has the same dependence on N_s as does the measured mobility, and is larger by about a factor of 2. Since there is no adjustable parameter in the calculation, the agreement is quite good.

An excellent review on electronic properties of

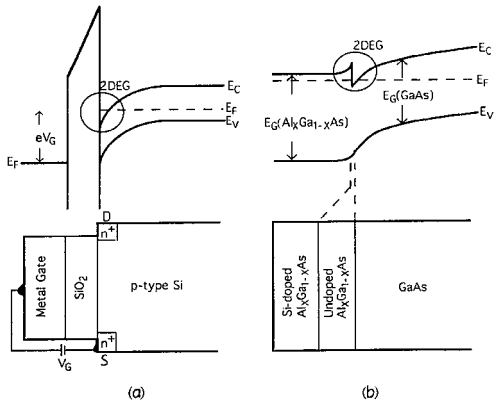

Fig. 4. Schematic structure and energy level diagram (a) Si-MOSFET and (b) GaAs/$Al_xGa_{1-x}As$ heterostructure.[13)]

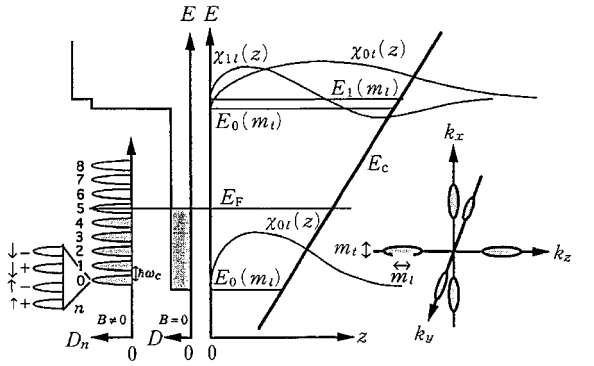

Fig. 5. Schematic energy level diagram of an n-channel inversion layer in a Si-MOSFET on a Si(001) surface. The bottom of the lowest 2D subband $E_0(m_\ell)$ arises from that $m_\ell \gg m_t$. D and D_n are density of states without and with a strong magnetic field perpendicular to the inversion layer. The Landau quantum number is denoted by n. Each Landau level with the same n splits into four Landau levels: ↑ and ↓ refer to parallel and antiparallel spin to the field, + and − refer to lower and higher valleys.[13)]

2DES is presented in 1982 by Ando, Fowler and Stern.[12)]

Here, the author introduces basic properties of the 2DES based on these articles.[11),12)] As shown in Fig. 4(a) on Si-MOSFETs, an insulator film (SiO_2) is sandwiched between a metal film, called the gate, and a silicon substrate. In an n-channel device, a current can flow between two heavily doped n^+-type contacts S and D, called the source and the drain, respectively, only when an n-type conduction layer (channel) is produced on the surface of p-type Si substrate adjacent to the SiO_2 film, by supplying a positive gate voltage V_G against the Si substrate which is usually in equillibrium with the source. The conduction layer is called the inversion layer because the conduction type is inverted from the substrate.

In a GaAs/$Al_xGa_{1-x}As$($x \simeq 0.3$) heterostructure system, called a HEMT (high electron mobility transistor),[14),15)] an n-type conduction layer is produced on the surface of undoped GaAs adjacent to a thin undoped GaAs/$Al_xGa_{1-x}As$ layer as shown schematically in Fig. 4(b).

The bottom of the conduction band of GaAs in the wave number space is a sphere; i.e. the conduction band is isotropic. However, the bottom of the conduction band in Si is anisotropic and consists of 6 ellipsoids of revolution along the ⟨100⟩ axis as shown in Fig. 5. Electron effective mass along the ⟨100⟩ axis m_ℓ and that in a plane perpendicular to the ⟨100⟩ axis m_t are given in unit of free electron mass m as $m_\ell = 0.916\,m$ and $m_t = 0.190\,m$ as schematically shown in Fig. 5. In the electrostatic potential in the inversion layer, the ground 2D subband $E_0(m_\ell)$ consists of two ellipsoids ($n_v = 2$) with $m_\ell = 0.916\,\mathrm{m}$ as schematically shown in Fig. 5. In the inversion layer on Si(111) surface, the valley degeneracy is considered to be 6, as 6 ellipsoids in the conduction band are equivalent.

As Stern and Howard[11)] described, three effective masses are necessary to describe the electronic properties of the inversion layer. One is m_3, the mass which determine energy levels $E_n(n = 0,1,2,-)$ for motion perpendicular to the surface. The other two, m_1 and m_2, are the principal effective masses of the constant energy ellipse associated with motion parallel to the surface. For (100) surface of Si, two of the six bulk constant-energy ellipsoids will give $m_3 = m_\ell$, the longitudinal effective mass of the bulk, while the other four will give $m_3 = m_t$, the transverse bulk effective mass. We list in Table 1 the values of masses m_1, m_2 and m_3 for the conduction band in the n-type inversion layer of Si for three high symmetry surface orientations, and in each case the valley degeneracy n_v is given for the number of ellipsoids of the bulk having equivalent set of values of electrons in the inversion layer. When two different values of m_3 are used, the solution of the Schroedinger equation belonging to the larger mass will have the lower energy level than the solution belonging to the smaller mass.

Table 1. Effective masses for three surface orientations for n-type silicon inversion layers.[11] $m_t = 0.190m_0$, $m_\ell = 0.916m_0$

Surface	m_1	m_2	m_3	n_v
(100)	m_t	m_t	m_ℓ	2
	m_t	m_ℓ	m_t	4
(110)	m_t	$(m_t + m_\ell)/2$	$(2m_t m_\ell)/(m_t + m_\ell)$	4
	m_t	m_ℓ	m_t	2
(111)	m_t	$(m_t + 2m_\ell)/3$	$(3m_t m_\ell)/(m_t + 2m_\ell)$	6

Stern and Howard[11] gives an approximate expression

$$g(z) = \frac{1}{2} b^3 z^2 exp(-bz) \quad [3]$$

for the charge distribution when only the lowest inversion layer energy level is occupied. The parameter b is given by a variational calculation as

$$b = ([48\pi e^2 m_3/\kappa_{sc}\hbar^2][N_{depl} + (11/32)N_s])^{1/3} \quad [4]$$

where N_{depl} and N_s are the concentration of charges in the depletion layer per square and the electron concentration in the inversion layer per square, respectively. The average value of z, weighted by the charge distribution given by Eq. [3], is $z_0 = 3/b$.

Stern and Howard[11] studied bound states in 2D systems. Their results for the most simple case are the following. If the electrons in the inversion layer have an isotropic effective mass $m* = m_1 = m_2$, if there were no screening by the inversion-layer electrons, if the inversion-layer charge distribution $g(z)$ were a delta function at the interface between the semiconductor and the insulator, and if the Coulomb center of charge e were also at the interface, then the effective potential energy would be

$$-e\bar{\phi}(r) = -e^2/\bar{\kappa}r \quad [5]$$

where

$$\bar{\kappa} = (\kappa_{sc} + \kappa_{ins})/2 \quad [6]$$

is the average of the dielectric constants in the semiconductor and the insulator. The solution of a 2D Schroedinger equation with the 2D potential given by Eq. [5] leads the eigenvalues of the infinite set of $(2n-1)$-fold degenerate levels

$$E_n = -(n - 1/2)^{-2} Ry^* \quad [7]$$

where the unit of energy is the effective Rydberg

$$Ry^* = m^* e^4/(2\bar{\kappa}^2\hbar^2) \quad [8]$$

and the quantum number n takes on the values $0, 1, 2, \ldots$. The ground state envelope function is

$$\psi = (8/\pi)^{1/2} a*^{-1}\, exp(-2r/a^*) \quad [9]$$

where

$$a^* = \bar{\kappa}\hbar^2/m^* e^2 \quad [10]$$

is the effective Bohr radius.

The numerical values of z_0, a^*, and Ry^* are given by Ando, Fowler and Stern[12] as

$$z_0(\mathrm{nm}) = 2.283\left(\frac{10^{12}\,\mathrm{cm}^{-2}}{N^*}\right)^{1/3}\left(\frac{\kappa_{\mathrm{sc}}}{11.5}\right)^{1/3} \times \left(\frac{0.916\mathrm{m}_0}{m_3}\right)^{1/3} \quad [11]$$

$$a^*(\mathrm{nm}) = 3.203\left(\frac{\kappa_{\mathrm{sc}}}{11.5}\right)\left(\frac{0.19m_0}{m^*}\right) \quad [12]$$

$$Ry^*(\mathrm{meV}) = 43.60\left(\frac{m}{0.19m_0}\right)\left(\frac{7.7}{\bar{\kappa}}\right)^2 \quad [13]$$

where $N^* = N_{depl} + (11/32)N_s$, and $7.7 = (\kappa_{sc} + \kappa_{ins})/2$ in a Si-MOSFET.

In the following, the author describes the progress in experimental research into the understanding of the quantum transport in surface and interface channels carried out in Gakushuin University over the last forty years in which the author was personally involved. To begin with, structures of samples of the 2DES are shown in Fig. 6 which shall be used for measurements of the transport properties of the 2DES in the following sections.

In the next section, a two-dimensional semiconductor which has a two-dimensional conduction band and two-dimensionally distributed donor atoms is described. Then two-dimensional electron systems in weak magnetic fields which brought us the birth of the quantum transport in a 2DES at low temperatures are described. In Section 3, a metal-insulator transition is described. In Section 4, two-dimensional electron systems in strong magnetic fields including the quantum Hall effect (QHE) are described. In Section 5, high precision meaurements of the quantized Hall resistance and new international electrical reference standard based on the QHE are described. In Section 6, experiments on activation energies in 1/3 and 2/3 fractional quantum Hall effects (FQHE) are described. In

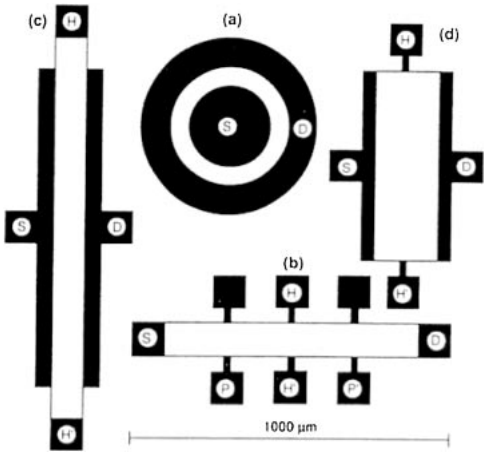

Fig. 6. Four examples of electrode structures of 2-dimensional electron systems with freedom in the xy-plane and a magnetic field in z-direction. Electrode S and electrode D in each sample, are the source-eletrode and the drain-electrode, respectively. Sample (a) is a Corbino disk which can measure directly the diagonal conductivity σ_{xx}. Sample (b) is a long Hall bar for Hall voltage measurement by two Hall electrodes, H and H′. Sample (c) is a wide Hall current bar for Hall current measurement by shorting two Hall electrodes H and H′. Sample (d) is a short Hall bar for measurements of Hall voltage and conductance.[13)]

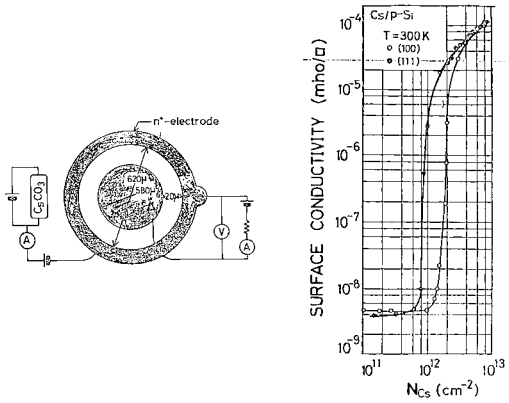

Fig. 7. A naked Corbino disk with a source- and a drain-electrode on a Si and a Cs_2CO_3 source (left). Surface conductivity increases with the adsorption of Cs atoms (right).[16)]

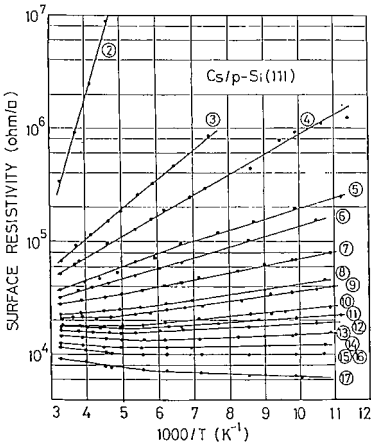

Fig. 8. Temperature dependence of the surface resistivity in a Cs-adsorbed p-type Si surface.[17)] Adsorbed Cs atom concentrations $N_{Cs}(10^{12}\,cm^{-2})$ for the sample number 2, 5, 10, and 17 in the circles are 1.0, 2.1, 3.5 and 8.0 respectively.

Section 7, breakdown of the QHE and collapse of the quantized Hall resistance are described. Concluding remarks are given in the final section.

2. Two-dimensional electron systems in weak magnetic fields

2.1. A two-dimensional semiconductor with a two-dimensional conduction band and donor atoms in a plane. A two-dimensional (2D) semiconductor with a 2D conduction band and a 2D plane of donors was studied by Kawaguchi.[16)] He used an n-channel Si-MOSFET with a Corbino disk electrode structure as shown in Fig. 6(a). He etched off a metal gate-electrode and a subsequent oxide film as shown in Fig. 7(left), and evaporated Cs atoms on the naked Si Corbino disk by heating a cesium carbonate film on a tungsten filament in vacuum. Then the conductance on the Si surface between the source- and the drain-electrode increases with the increase in the adsorption of Cs atoms as shown in Fig. 7(right). The surface conductance increases rapidly at $N_{Cs} \sim 8 \times 10^{11}\,cm^{-2}$ in a (111) Si surface and at $N_{Cs} \sim 1.5 \times 10^{12}\,cm^{-2}$ in a (100) Si surface. These behaviors of the surface conductance of Si against the increase in adsorbed Cs atoms can be explained by a following process.

On an etched Si surface, there are surface energy levels arised from broken chemical bonds. Cs donor levels appear above these surface levels. Electrons in the adsorbed Cs atoms fill at first the surface levels arised from the broken surface bonds. Then electrons are thermally activated to the conduction band in the Si surface inversion layer. Temperature dependence of the surface resistivity with adsorbed Cs atoms shows thermally activated conduction as shown in Fig. 8. Figure 8 shows that the activation energy of the adsorbed Cs atoms E_{Cs} decreases with the increase in the number of

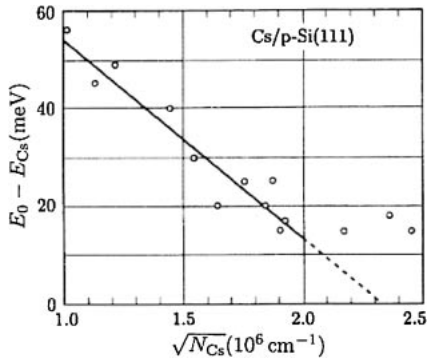

Fig. 9. Adsorbed Cs atom concentration dependence of the activation energy of surface resistivity in a Cs-adsorbed p-type Si surface.[16)]

adsorbed Cs atoms N_{Cs}.

It is well known by Pearson and Bardeen's classic experiment[18)] that the activation energy E_A of acceptor atoms in p-type Si decreases with the increase in acceptor concentration N_A as expressed by $E_A = E_{I0} - aN_A^{1/3}$ where E_{I0} is the ionization energy of an isolated acceptor. Their result in a 3-dimensional system shows that the activation energy of acceptors has a decreasing term which is inversely proportional to the average distance between acceptor atoms.

In the present 2D system which consists of a 2-dimensional conduction band in an n-type inversion layer on a p-type Si surface and 2-dimensionally distributed Cs donors on the surface, it is expected that the activation energy of Cs donors has a decreasing term which is inversely proportional to the average distance between Cs atoms.

As shown in Fig. 9, the activation energy in the present 2D system is given by

$$E_{Cs} = E_{I0} - bN_{Cs}^{1/2} \qquad [14]$$

where E_{I0} is the ionization energy of an isolated donor in the 2DES and the $bN_{Cs}^{1/2}$ is the term inversely proportional to the average distance between Cs atoms. A straight line is given by $E_{Cs}(\text{meV}) = 96 - 4.1 \times 10^{-5} N_{Cs}(\text{cm}^{-2})^{1/2}$.

When we use $\bar{\kappa} = (11.8 + 1)/2 = 6.4$ and the density of state mass for m^* as $m^* = \sqrt{(m_1 m_2)} = \sqrt{(m_t(m_t + 2m_\ell)/3)} = 0.358 m_0$ for a 2DES in Si(111) surface inversion layer, we have $a^* = 9.5\,\text{A}$, $Ry^* = 119\,\text{meV}$ and Eq. [7] for $n = 0$ leads $E_{I0} = 4Ry^* = 476\,\text{meV}$. Experimental result of E_{I0} is $E_{I0}(\text{exp}) = 96\,\text{meV}$. In the case when there is a distance d between the 2DES and a donor, the binding energy of a donor is reduced. Stern and Howard[11)] calculated numerically the effect of distance between the 2DES and charged centers and effect of screening. Following the result in Fig. 5 in Stern and Howard's paper,[11)] we have $E_{I0} = 0.8Ry^* = 95\,\text{meV}$ for the case $d = 1.3a^*$ without screening effect. The result explains the present experimental result.

The present experimental result is a 2D version of the activation energy which depends on the impurity concentration observed for Si bulk semiconductors as $E_I = E_{I0} - aN_I^{1/3}$ by Pearson and Bardeen,[18)] where E_I is the activation energy of donors and acceptors whose concentration is given by N_I. Thus, the Cs-adsorbed Si surface is considered to be a 2D semiconductor with a 2D conduction band and two-dimensionally distributed donors.

2.2. Quantum transport in a 2DES in weak magnetic fields: weak localization in silicon inversion layers. In 1978, Kawaguchi, Kitahara and Kawaji[19)] carried out experiments on a 2DES in the metallic conduction in Cs-adsorbed Si surfaces which show interesting transport properties at low temperatures as shown in Fig. 10. Temperature dependence of the resistivity in Fig. 10(a) is described by $\rho(T) = a - b\log T$. The resistivity decreases with a magnetic field applied perpendicular to the 2D plane (negative magnetoresistance) as shown in Fig. 10(b).

The 2-dimensional nature of the negative magnetoresistance in the 2DES can be more clearly shown by the angle dependence of the magnetic field observed in the Si-MOS(111) inversion layer shown in Fig. 11. The results of an experiment carried out in 1984 for a 2DES in a GaAs/AlGaAs heterostruc-

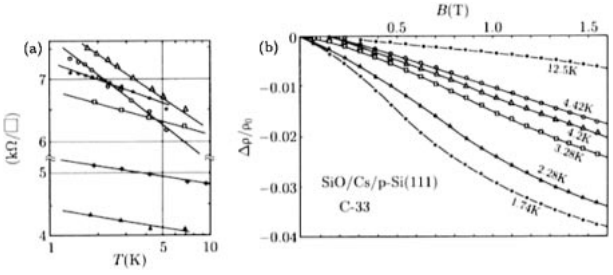

Fig. 10. Experimental results in Cs-Si(111) n-channel inversion layers at low temperatures.[19)] (a) Temperature dependence of resistivity. (b) Magnetic field dependence of negative magnetoresistance.

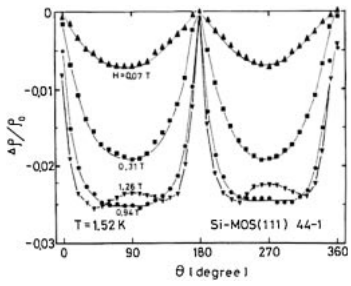

Fig. 11. Angular dependendence of the negative magnetoresistance in a Si-MOS(111) inversion layer where $\theta = 0$ at $B \parallel$ surface and $\theta = 90°$ at $B \perp$ surface.[20)]

ture also show clearly the 2D nature of the negative magnetoresistance (see also Fig. 16).

Understanding of the experimental results shown by Figs. 10 and 11 was made possible by weak localization effect in a 2DES. A theoretical framework for weak localization including a magnetic field effect on the weak localization was established in 1979.[21)–28)] Characteristic properties of the weak localization in normal 2D systems are the following: (1) The conductivity decreases with decreasing temperature T with a term proportional to $logT$, and (2) an external magnetic field perpendicular to the 2D system increases the conductivity.

The scaling theory of localization by Abrahams, Anderson, Licciardello and Ramakrishnan[22)] derived that the conductivity σ in the weakly localized regime where $\epsilon_F \tau/\hbar \gg 1$, ϵ_F and τ being the Fermi energy and elastic scattering time, respectively, is given with a correction term $\Delta\sigma_L$ by

$$\sigma = \sigma_0 + \Delta\sigma_L. \qquad [15]$$

Here $\sigma_0 = N_s e^2 \tau/m^*$ is the Drude conductivity.

We summarize here a temperature dependent correction term for the conductivity in the weak localization in a 2DES following Anderson, Abrahams and Ramakrishnan[23)] as given by

$$\Delta\sigma_L(T) = \frac{\alpha p e^2}{2\pi^2\hbar} log\mathrm{T} \qquad [16]$$

where α is a numerical constant and p is the exponent in the temperature dependence of the inelastic scattering time τ_ϵ given by

$$\tau_\epsilon(T) \propto T^{-p}. \qquad [17]$$

We note here that the Si conduction band consists of six equi-energy ellipsoids in k-space ($n_v = 6$. See Fig. 5). Therefore, α in Eq. [16] should be replaced by $n_v\alpha$ when the inter-valley scattering time τ_i is longer than the inelastic scattering time τ_ϵ.

The $logT$ dependent electrical resistivity in Fig. 10(a) leads the coefficient $\alpha p = 0.98$ in Eq. [16] for the sample in the upper most line given by open triangles and $\alpha p = 0.81$ for the sample in the lower most line given by filled triangles. The present 2DES is electrons in an n-type inversion layer on a Si(111) surface. Therefore, the coefficient αp should be given by $n_v \alpha p$ where n_v is the valley degeneracy.[29),30)] However, if the inter-valley scattering time of the electrons is shorter than the inelastic scattering time, the number n_v should be given as $n_v = 1$. Thus, we can understand that $n_v \alpha p \simeq 1$ in the 2DES in n-channel Si inversion layers.

In 1980, Bishop, Tsui and Dynes[31)] reported their result of the $logT$ dependent electrical resistivity in an n-channel Si inversion layer of a Si-MOSFET on a Si(100) surface observed at low temperatures $0.1\,\mathrm{K} < T < 1\,\mathrm{K}$ and found that $\alpha p/2 = 0.51 \pm 0.05$. Their result has also shown that $n_v \alpha p \simeq 1$ which gives that the intervalley scattering time is much shorter than the inelastic scattering time τ_ϵ.

Hikami, Larkin and Nagaoka[25)] derived explicit expressions of negative magnetoresistance for the cases which include the spin-orbit scattering and magnetic scattering by impurity spins in a 2DES. Their theory gives the change in the conductivity of a 2DES by application of a magnetic field B as

$$\Delta\sigma_{\mathrm{HLN}}(B) = \frac{n_v \alpha e^2}{2\pi^2\hbar}\left[\Psi\left(\frac{1}{2}+\frac{1}{a\tau_\epsilon}\right) - \Psi\left(\frac{1}{2}+\frac{1}{a\tau}\right) + \log\frac{\tau_\epsilon}{\tau}\right] \qquad [18]$$

where Ψ is the Digamma function and $a = 2DeB/h$ for the diffusion coefficient of electrons D. Here, $a\tau$ is given by the electron mean free path ℓ and the radius of the ground Landau orbit $\ell_B = \sqrt{(\hbar/eB)}$ as

$$a\tau = \frac{2\ell^2}{\ell_B^2} = \frac{\sigma_0(\mathrm{mho})\mu\mathrm{B}}{1.93\times10^{-5} n_v}. \qquad [19]$$

Experimental results obtained for a Si-MOSFET by Kawaguchi and Kawaji[32)] were well explained by Hikami, Larkin and Nagaoka's theory expressed by Eq. [18][25)] as shown by the magnetic field dependences of $\Delta\sigma(B)$ at 4.2 K and 12.1 K in the left in Fig. 12, and a temperature dependence of the

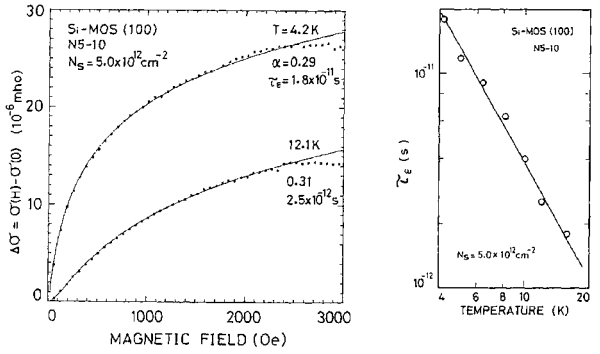

Fig. 12. Left: Magnetic field dependence of the magnetoconductivity of a Si-MOSFET.[32] Experimental data (dots) are fitted to Hikami, Larkin and Nagaoka's theory.[25] Right: Temperature dependence of the inelastic scattering time τ_ϵ extracted from the magnetoconductivity.[32]

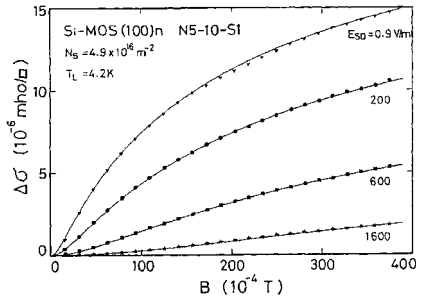

Fig. 13. Magnetic field dependence of the change in the conductivity $\Delta\sigma(B)$ of a high mobility Si(100) MOSFET inversion layer for different source-drain electric field E_{SD}.[34]

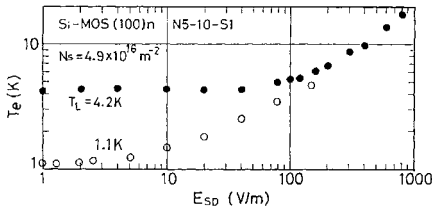

Fig. 14. Source-drain electric field dependence of the electron temperature in a high mobility Si(100) MOSFET inversion layer at two lattice temperatures measured by negative magnetoresistance effect.[34]

inelastic scattering time τ_ϵ in the right in the same figure. See also an article.[33]

2.3. Measurements of electron temperature and electron-phonon interaction in 2DES in Si-MOSFETs. The negative magnetoresistance in the weak localization of electrons is controlled by inelastic scattering. The inelastic scattering time τ_ϵ has a strong temperature dependence as given by $\tau_\epsilon \propto T^{-p}, 1 \leq p \leq 3$. Therefore, the inelastic scattering time can be used as a thermometer for the temperature of electrons in non-equillibrium with the lattice.

Kawaguchi and Kawaji[34] applied the negative magnetoresistance effect to measurement of electron temperature in Si-MOS inversion layers at high electric fields for evaluating the deformation potential constants in electron-phonon interaction. As will be discussed later, the inelastic scattering at liquid helium temperatures refers to electron-electron scattering. Therefore, we can estimate electron temperature of the 2DES in a thermally nonequilibrium state with the lattice by τ_ϵ extracted from the negative magnetoresistance data.

Figure 13 shows the magnetoconductivity of a Si(001) MOS inversion layer with peak mobility of $11{,}000\,\mathrm{cm^2/V{\cdot}s}$ at 4.2 K at various source-drain field E_{SD} at lattice temperature T_L of 4.2 K. Similar magnetoconductivity measurements were made at $T_L = 1.1$ K. The inelastic scattering time τ_ϵ is determined from the magnetoconductivity at different E_{SD} by use of the HLN theory (Eq. [18]). The electron temperature T_e at different E_{SD} is evaluated from the T-dependence of τ_ϵ measured at $E_{SD} = 1\,\mathrm{V/cm}$. Then, E_{SD}-dependence of the electron temperature T_e at two lattice temperatures $T_L = 4.2$ K and $T_L = 1.1$ K are shown in Fig. 14. At $T_L = 4.2$ K, the change in the electron temperature due to the variation in E_{SD} between 40 V/m and 800 V/m is about 14 K. For this change in the electron temperature, the inelastic scattering time changes almost one order of magnitude as shown in Fig. 12.

In a stationary state at a high source-drain field, the rate of energy gain per electron from electric field, $\sigma_0 E_{SD}^2/N_s$, is equal to the rate of energy loss to the lattice system, $-d\epsilon/dt$. The energy loss per electron from the electron system to the lattice by electron-surfon scattering[35] was calculated by Shinba *et al.* (see the reference 34 and the reference 36) by using the deformation potential constants of bulk silicon, $\Xi_u = 12\,\mathrm{eV}$, $D = \Xi_d/\Xi_u = -0.67$. Figure 15 shows the experimental data of $\sigma_0 E_{SD}^2/N_s$ (open and solid circles) and calculated value of $-d\epsilon/dt$ (solid lines) as a function of $(T_e - T_L)$. Agreement between theoretical results and experimental results shows that the deforma-

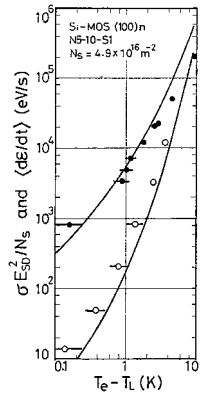

Fig. 15. T_e (electron temp.) $-$ T_L (lattice temp.) dependence of energy gain per electron $\sigma E_{SD}^2/N_s$ from the source-drain electric field E_{SD} measured at $T_L = 4.2$ K (filled circles) and at $T_L = 1.1$ K (open circles) measured in a high electron mobility Si(100) MOSFET and the energy loss per electron to the lattice $-(d\epsilon/dt)$ calculated by Shinba and Nakamura (See the ref. 36).

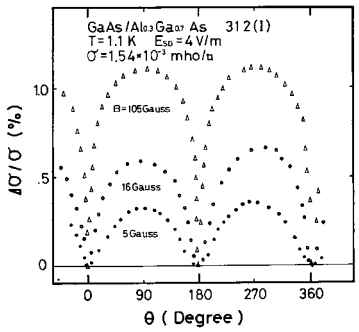

Fig. 16. A 2DES in GaAs/Al_xGa_{1-x}As heterostructure shows clearly two-dimensional nature of the negative magnetoresistance in the angle dependence of the change in the conductivity in magnetic fields.[39),46)]

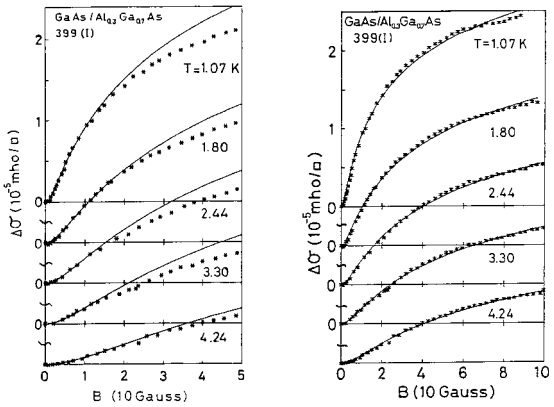

Fig. 17. Left: Magnetic field dependence of the magnetoconductivity of a GaAs/Al_xGa_{1-x}As($x \simeq 0.3$) 2DES.[39),43),46)] Numerical errors in the ordinate in Fig. 4 in Ref. 39 have been corrected in this figure. Experimental data (dots) are fitted to Hikami, Larkin and Nagaoka's theory.[25)] Right: Magnetic field dependence of the magnetoconductivity of a GaAs/Al_xGa_{1-x}As($x \simeq 0.3$) 2DES.[43),46)] Experimental data (dots) are fitted to Kawabata's theory.[41)]

tion potential constants in the inversion layer are almost the same as the silicon bulk values.

2.4. Further studies on quantum transport in weak localization in 2DES in GaAs/ $Al_xGa_{1-x}As(x \simeq 0.3)$ heterostructures. The electron system in an GaAs/Al_xGa_{1-x}As($x \simeq 0.3$) heterostructure interface is the simplest 2DES if N_s is sufficiently small to maintain single 2D subband. In particular, in order to make clear understanding of the inelastic scattering time, measurements of the negative magnetoresistance in the GaAs/ Al_xGa_{1-x}As 2DES are necessary by following reasons: (1) The present system is free from the intervalley scattering effect ($n_v = 1$). (2) The spin Zeeman effect is small due to the small g-factor of the conduction electrons. (3) The mutual interaction effect can be minimized by analysing the magnetic field dependence of the conductivity at the weak field limit. However, experimental studies so far carried out on the weak localization have not necessarily derived reasonable results.[37),38)]

Nambu *et al.*[39)] made careful measurements of magnetoconductivity in 2DES in GaAs/ $Al_xGa_{1-x}As(x \simeq 0.3)$ heterostructures with low electron mobilities. Angular dependence of magnetoconductivity in Fig. 16 shows that the present system is an ideal 2DES for the study of the weak localization.

Nambu *et al.*[39)] employed samples with low elecron mobilities such as μ(sample 399(I)) = 2.1 m^2/V·s and μ(sample 354A(B)) = 4.1 m^2/V·s. Experimental magnetoconductivity data are fitted to Hikami, Larkin and Nagaoka's formula with $n_v\alpha = 1$ given by Eq. [18] in the magnetic field region lower than 10 Gauss ($a\tau < 0.15$) as shown in Fig. 17(Left). They discussed their experimental results of τ_ϵ based on the theoretical results by Fukuyama and Abrahams.[40)]

In 1984, Kawabata[41)] developed a theory of negative magnetoresistance in a 2DES which is a two-dimensional version of his theory of negative magnetoresistance in three dimensional systems presented in 1980.[42)]

As shown by Kawabata,[41] Hikami, Larkin and Nagaoka theory (HLN thoery) for negative magnetoresistance in 2DES is correct when the relation

$$\omega_c\tau \ll \hbar/\epsilon_F\tau \ll 1 \qquad [20]$$

is fulfilled where ω_c, ϵ_F and τ are cyclotron frequency, Fermi energy and momentum relaxation time of electrons. Since the parameter $\hbar/\epsilon_F\tau$ must be small enough in order that the weak localization theory is correct, HLN theory is applicable only to the regions of very weak magnetic field.

Kawabata's theory[41] is valid when the condition

$$\omega_c\tau, \hbar/\epsilon_F\tau \ll 1, \qquad [21]$$

is fulfilled. This condition is applicable to much wider region of magnetic field where $a\tau \leq 1$ than HLN theory.

Nambu *et al.*'s experimental results of magnetoconductivity were fitted to Kawabata's theory in a wide magnetic field region as shown in Fig. 17(Right) where we have $a\tau = 1$ near the maximum field.

The temperature dependence of the inelastic scattering time τ_ϵ extracted from the field dependence of the magnetoresistance is shown by open circles in Fig. 18.[43),44] In Fig. 18, the theoretical results of the inelastic scattering time τ_ϵ(th)[43] is calculated based on Fukuyama and Abrahams.[40] Agreement between the inelastic scattering time extracted from experimental results by Kawabata's theory shown by ○ and the theoretical results τ_ϵ(th) shown by △ is excellent.

Kawabata's theory is also applied to fit magnetoconductivity data in Si 2DES.[45]

Other topics and future problems are discussed in 1986.[46]

3. Metal-insulator transition in 2DES in Si-MOSFETs and spin-degree of freedom

A Si-MOSFET is an interesting 2DES whose electron concentration can be controlled between zero and about $10^{17}\,\mathrm{m}^{-2}$ by application of a gate voltage. One of the interesting phenomena observed in this system is a metal-insulator transition (MIT) which occurs at a finite concentration of electrons in a 2DES.

Okamoto *et al.*[47] have clearly observed an important role of the spin degree of freedom in the MIT in a Si-MOSFET. In Fig. 19, the diagonal resistivity ρ_{xx} of a high electron mobility 2DES ($\mu_{max} = 2.4\,\mathrm{m}^2/\mathrm{V{\cdot}s}$) in a Si-MOSFET is shown at five temperatures between $T = 0.31\,\mathrm{K}$ and $T = 1.32\,\mathrm{K}$ for different electron concentrations N_s. In zero magnetic field, no temperature dependence is observed in the resistivity ρ_{xx} at $N_\mathrm{s} \simeq 1\times10^{15}\,\mathrm{m}^{-2}$. In the lower N_s region, $N_\mathrm{s} < 1\times10^{15}\,\mathrm{m}^{-2}$, the resistivity increases with decreasing temperature. In the higher N_s region, $N_\mathrm{s} > 1\times10^{15}\,\mathrm{m}^{-2}$, the resistivity decreases with decreasing temperature. The critical value of ρ_{xx} at the MIT is $55\,\mathrm{k}\Omega$. This value is close to $\rho_c \sim 2h/e^2$ reported by Kravchenko *et al.*[48] When a magnetic field, $B = 9\,\mathrm{T}$, is applied

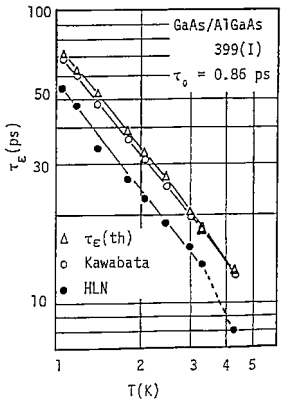

Fig. 18. Temperature dependence of the inelastic scattering time in a GaAs/AlGa$_x$As$_{1-x}$ heterostructure interface.[43),44] ○: τ_ϵ determined by Kawabata's theory in Fig. 17(Right). ●: τ_ϵ determined by Hikami, Larkin and Nagaoka's theory in Fig. 17(Left). △: calculated τ_ϵ(th).[43),46]

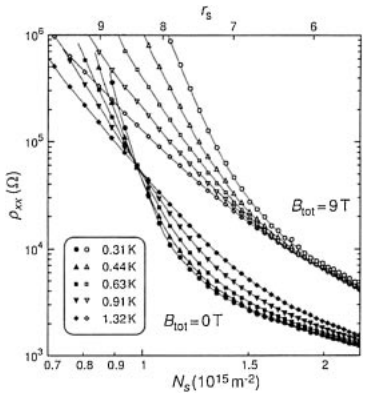

Fig. 19. Diagonal resistivity as a function of electron concentration for different temperatures in a zero magnetic field (closed symbols) and in a magnetic field of $B = 9\,\mathrm{T}$ applied parallel to the 2D plane.[47]

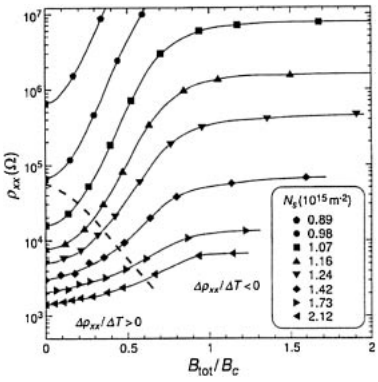

Fig. 20. Resistivity ρ_{xx} vs $B_{\rm tot}/B_c$ at $T = 0.21\,\mathrm{K}$ and $B_\perp = 0$ for various N_s. The dashed line represents the critical value of ρ_{xx} at the MIT determined from temperature dependence between 0.21 and 0.91 K.[47)]

parallel to the 2D plane, the resistivity increases with the decrease in the temperature in the whole $N_{\rm s}$ region in this figure or the metallic phase disappears. The disappearance of the metallic phase is caused by the Zeeman splitting effect of the conduction electrons.

Figure 20 shows magnetic field dependences of the resistivity ρ_{xx} of the 2DES in the Si-MOSFET used in Fig. 19 measured at $T = 0.21\,\mathrm{K}$ for different electron concentrationsions $0.89 \times 10^{15}\,\mathrm{m}^{-2} \leq \mathrm{N_s} \leq 2.12 \times 10^{15}\,\mathrm{m}^{-2}$. Here, the magnetic field is applied parallel to the 2D plane and the unit $B_{\rm c}$ is the critical magnetic field where the spin polarization p reaches $p = 1$. The critical magnetic field $B_{\rm c}$ is described in detail by Okamoto *et al.*[47)] The diagonal resistivity ρ_{xx} increases with $B_{\rm tot}$ in the low-$B_{\rm tot}$ region, but it takes almost constant values in the high-$B_{\rm tot}$ region. The saturation of ρ_{xx} occurs around $B_{\rm tot} = B_{\rm c}$ at which the polarization is expected to be completed. The result indicates that the mixing of the different spin states causes the reduction of ρ_{xx} in the low-$B_{\rm tot}$ region. The dashed line represents the critical value of ρ_{xx} at the MIT. It was tentatively determined by the sign of the change in ρ_{xx} from $T = 0.21$ to 0.91 K. The positive temperature dependence of ρ_{xx} below 1 K was not observed for $B_{\rm tot} > B_{\rm c}$. The positive T dependence of ρ_{xx} in the low $B_{\rm tot}$ region may arise from the scattering related to the spin degree of freedom.

Suppression of the metallic behavior by a strong magnetic field applied parallel to the 2D plane has been reported for 2D hole systems in GaAs/AlGaAs heterostructures.[49)]

Okamoto *et al.*[50)] measured magnetotransport on a silicon 2D system in a Si/SiGe quantum well with a mobility two orders higher than Si-MOS samples. In this system, the metallic behavior remains even in an in-plane magnetic field. In the 2D hole systems in GaAs/AlGaAs heterostructures, the internal degree of freedom is spin only. However, the internal degree of freedom of valleys in Si conduction band remains in a 2D electron system in a Si-quantum well when a strong magnetic field is applied parallel to the 2D plane. Okamoto *et al.* have proposed a schematic phase diagram for T-dependence of ρ in low-resistivity and strongly correlated 2D systems in a plane disorder vs $g_{\rm s}g_{\rm v}$ where $g_{\rm s}$ is the spin degree of freedom and $g_{\rm v}$ is the valley degree of freedom.

4. Two-dimensional electron systems in strong magnetic fields

4.1. Landau levels and Anderson localization in 2DES in strong magnetic fields. When a strong magnetic field B is applied in z-direction in a 2DES in xy plane as shown in Fig. 5, the energy levels of the 2DES are quantized to Landau levels given by

$$\epsilon_n = \left(n + \frac{1}{2}\right)\hbar\omega_c, \quad n = 0, 1, 2 - - \qquad [22]$$

where $\omega_c = eB/m*$ is the cyclotron angular frequency of an electron. The radius of the cyclotron motion of an electron with the Landau quantum number n is given by

$$\ell_n = \sqrt{(2n+1)}\ell_B \qquad [23]$$

where $\ell_B = \sqrt{(\hbar/eB)}$ is the radius of the cyclotron orbit of an electron in the ground Landau level. Degeneracy of a Landau level is given by

$$N_{\rm L} = \frac{eB}{h} \qquad [24]$$

as a product of the density of states $D_2(g_s = 1, g_v = 1)$ and the Landau level splitting $\hbar\omega_c$.

Quantities given in Table 2 (Table 1 in the references 13, 43) show that 1 K is low enough temperature to realize the extreme quantum-limit condition in an n-channel Si(001) MOS inversion layer in the field of 10 T so far as the separation of Landau levels with different Landau quantum number is concerned. A schematic energy level diagram of an n-channel inversion layer in a

Table 2. Quantities related to transport properties in 2DES in an n-channel Si(001) inversion layer and an n-channel GaAs inversion layer in a strong magnetic field. The radius of the ground Landau orbit is given by $\ell_0(\mathrm{A}) = 256.6/B(\mathrm{T})^{1/2}$ and the degeneracy of a Landau level is given by $eB/h(\mathrm{m}^{-2}) = 2.418 \times 10^{14} B(\mathrm{T})$

Quantity	Si(001)	GaAs
$\hbar\omega_c(\mathrm{K})/B(\mathrm{T})$	7.070	19.75
$\Gamma_{\mathrm{SCBA}}(\mathrm{K})[\mu(\mathrm{m}^2/\mathrm{Vs})/B(\mathrm{T})]^{1/2}$	5.642	15.76
$\Gamma_\tau(\mathrm{K})\mu(\mathrm{m}^2/\mathrm{Vs})$	3.536	9.880
$g\mu_{\mathrm{B}}(\mathrm{K})/B(\mathrm{T})$	1.344	0.349

Si-MOSFET on a Si(001) surface is shown in Fig. 5. An n-channel inversion layer in GaAs/$\mathrm{Al}_x\mathrm{Ga}_{1-x}\mathrm{As}(x \approx 0.3)$ heterostructure interface is more easy to realize the extreme-quantum-limit condition than Si-MOSFET as the structure of the conduction band in GaAs is simple and the electron effective mass is small.

By use of a Corbino disk, Kawaji and Wakabayashi[51] have performed careful experiments on the finite gap regions in the gate voltages for the vanishing σ_{xx} with various source-drain electric fields and investigated the magnetic field dependence and the Landau level index dependence of the concentration of immobile electrons or localized electrons. The diagonal conductivity σ_{xx} in a Si-MOSFET in $B = 14\,\mathrm{T}$ at $T = 1.4\,\mathrm{K}$ for various source-drain electric fields is shown in Fig. 21. The magnetic field dependence of the width of the gate voltage for the vanishing conductivity region ($\sigma_{xx} < 10^{-9}$ mho) has shown that the sum of the concentration of immobile or localized electrons associated with the higher edge of the $(n-1)$-th Landau level and the lower edge of the n-th Landau level, where n is the Landau level quantum number, is approximately given by $[2\pi\ell_B^2(2n+1)]^{-1}$ as shown in Fig. 22 where ℓ_B is the radius of the ground Landau orbit. This result means that the electron wave functions become extended or pinned correlated states become free when the whole area of the inversion layer is covered by cyclotron orbits with radius of $(2n+1)^{1/2}\ell_B$.

In such a system in the extreme-quantum-limit condition, there exist gap regions in the density of states between the boundary of each Landau level. When random potentials are incorporated in the system, localized states are expected to exist near lower and higher edges of each Landau level. If the range of the random potential δ is much longer than

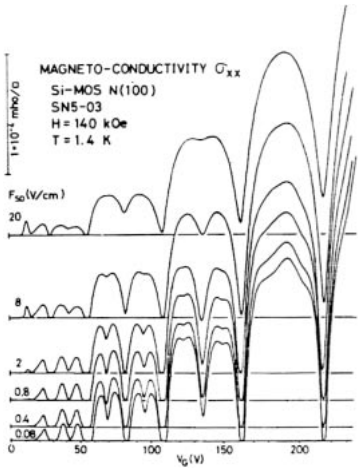

Fig. 21. Gate voltage dependence of the diagonal conductivity σ_{xx} of a Si(001) MOS inversion layer in $B = 14\,\mathrm{T}$ at $T = 1.4\,\mathrm{K}$ for various source-drain fields F_{SD}.[51]

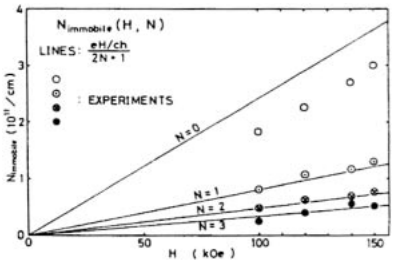

Fig. 22. Magnetic field dependence of the concentration of immobile electrons associated with the higher edge of the (N-1)-th Landau level and the lower edge of the Nth Landau level.[51] N = n in this figure.

the radius of a Landau orbit $\ell_n = \ell_B(2n+1)^{1/2}$, it is easy to see that centers of Landau orbits near the bottoms and tops of the random potentials move along closed trajectories lying in equi-potential lines. When the range of the random potentials is short ($\delta < \ell_n$), they also produce localized states near the lower and higher edges. These localized states exhibit exponential localization. Extended states which exist near the center of each Landau level are expected to show a different behavior from those in the absence of magnetic fields.

The first experiment of Shubnikov-de Haas effect in Si-MOSFETs by Fowler, Fang, Howard and Styles[8] has shown the existence of gap regions in the gate voltages where the diagonal conductivity σ_{xx} vanishes in strong magnetic fields. Fowler *et al.* employed samples of Corbino disks on

Si(001) MOS inversion layers for their measurements. As shown in Fig. 6, the Corbino disk is the only electrode structure for measurement of the diagonal conductivity σ_{xx} in any strength of magnetic field or in any value of the Hall angle from zero to $\pi/2$.

Kawaji and Wakabayashi measured temperature dependence of σ_{xx} in the lower edge of the lowest Landau level in a Si(001) inversion layer in a MOSFET in a magnetic field $B = 9.75\,\mathrm{T}$ at temperatures between 1.5 K and 4.2 K and observed activation type temperature dependence.[52] They used a model to describe the experimental results based on a quantum diffusion of Schottky defects in a Wigner crystal in the 2DES.

4.2. Measurements of the Hall conductivity in a 2DES in strong magnetic fields. Ando, Matsumoto and Uemura[53] have developed a theory of Hall effect in a 2DES in strong magnetic fields. Their results at $T = 0$ are summerized as follows:

(1) The Hall conductivity σ_{xy} is given by

$$\sigma_{xy} = -\frac{N_s e}{B} + \frac{\Gamma}{\hbar\omega_c}\sigma_{xx} \qquad [25]$$

where Γ is the Landau level broadening.

(2) The Hall conductivity is not affected by the presence of impurities when each Landau level is completely filled and the Hall conductivity is given by

$$\sigma_{xy} = -\frac{ie^2}{h} \qquad [26]$$

when the Fermi level lies in energy gap between the ith and $(i+1)$-th Landau levels.

(3) In the case of impurity bands being separated from each Landau level, the Hall conductivity is given by Eq. [26] when the Fermi level lies in any spectral gap lying between the i-th and the $(i+1)$-th main Landau level, i.e. when the Fermi level lies in gaps between two impurity bands or between an impurity band and the main Landau level.

Schematic presentation of the theoretical results described above is shown in Fig. 23(a) with Ando's prediction of the quantized Hall conductivity in (b).

Igarashi, Wakabayashi and Kawaji[55,56] carried out measurements of the Hall effect in a strong magnetic field using a wide Hall bar in Fig. 6(d). From measured source-drain current I_{SD} and Hall voltage V_H, they derived the diagonal conductivity σ_{xx} and the Hall conductivity σ_{xy} by use of Wick's solution for the Hall electric field distribution.[57] Their experimental results in 9.8 T at 1.6 K approximately confirmed Ando *et al.*'s theoretical results. However, the observed difference between $N_s e/B$ and $-\sigma_{xy}$ is much larger than $\sigma_{xx}\Gamma/\hbar\omega_c$ where Γ is calculated by Ando and Uemura's result of self-consistent Born approximation.[58] Wakabayashi and Kawaji[59] made further measurements of the Hall conductivity and the diagonal conductivity in a strong magnetic field using a long Hall bar in Fig. 6(b). However, discrepancy exists between the experimental results and theoretical results by Ando *et al.*[53]

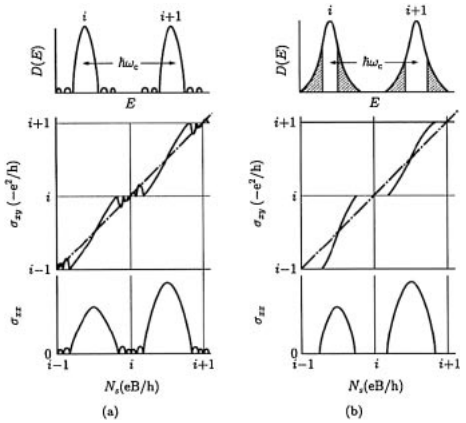

Fig. 23. (a) Schematic presentation of theoretical results of the Hall conductivity and the diagonal conductivity versus the filling factor of Landau levels by Ando, Mtsumoto and Uemura.[53] (b) Ando's prediction of the quantized Hall conductivity and the localization of electrons in Landau levels.[54]

By employing the Hall current method using a wide Hall current bar, the sample (c) in Fig. 6, Wakabayashi and Kawaji[60] have first confirmed experimentally Ando *et al.*'s result (1) for the Hall conductivity as described in the following.

The Hall current bar has the length between the source electrode and the drain electrode $L = 100\,\mu\mathrm{m}$. The width of these electrodes is $W = 1000\,\mu\mathrm{m}$ and the distance between two Hall current electrodes is $W_0 = 1200\,\mu\mathrm{m}$. In the Hall current method, they keep a constant source-drain voltage V_{SD} and measured the source-drain current I_x and the Hall current I_y between short-circuited Hall current electrodes H and H′. By employing Wick's method,[57] they calculated h^* function and

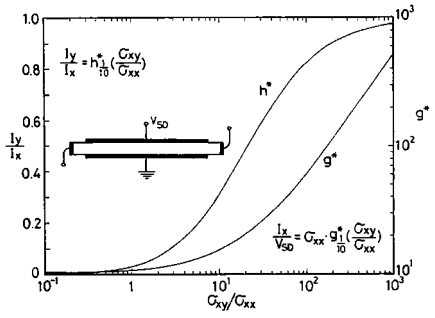

Fig. 24. Wick's h^* function in Eq. [27] and g^* function in Eq. [28] calculated against σ_{xy}/σ_{xx} for the Hall current bar with the length $L = 100\,\mu\text{m}$, the width $W = 1000\,\mu\text{m}$ and the distance between two Hall current electrodes $W_0 = 1200\,\mu\text{m}$.[60]

g^* function against $\tan\theta_{\text{H}} = \sigma_{xy}/\sigma_{xx}$ as shown in Fig. 24. These two functions lead the following two relations.

$$\frac{I_y}{I_x} = h^*_{L/W}\left(\frac{\sigma_{xy}}{\sigma_{xx}}\right) \qquad [27]$$

$$\frac{I_x}{V_{\text{SD}}} = \sigma_{xx} g^*_{L/W}\left(\frac{\sigma_{xy}}{\sigma_{xx}}\right). \qquad [28]$$

They determine σ_{xy}/σ_{xx} by use of measured value of I_y/I_x for the h^* function. They determine σ_{xx} by measured value of I_x/V_{SD} and $g^*_{L/W}(\sigma_{xy}/\sigma_{xx})$ using Eq. [28]. Then, they can determine σ_{xy}. Figure 25(a) shows experimental results of I_x and I_y as a function of V_{G} in a low mobility sample N9-8H53. Figure 25(b) shows σ_{xy} and σ_{xx} derived from (a). In the Fig. 25(b), a solid line in σ_{xx} is a result measured by a Corbino disk. A solid curve in σ_{xy} in Fig. 25(b) is a calculated result by Eq. [25] where Γ is replaced by Γ_{SCBA} which is calculated by

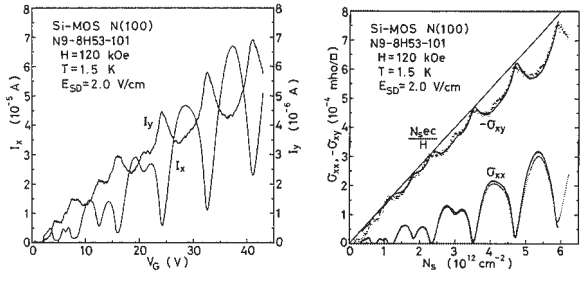

Fig. 25. (a) Measured source-drain current I_x and Hall current I_y in a sample N9-8H (peak mobility: $3800\,\text{cm}^2/\text{Vs}$), (b) the Hall conductivity σ_{xy} and the diagonal conductivity σ_{xx} determined from the results in (a) by Wick's method given by Eq. [27] and [28] and results in Fig. 24.[60]

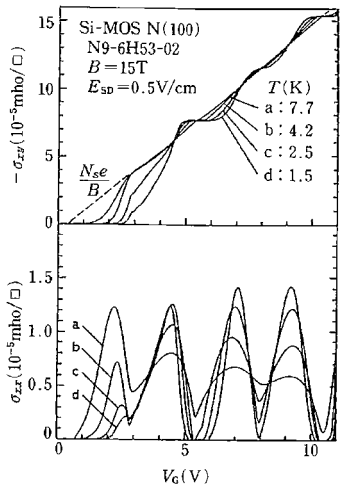

Fig. 26. Hall conductivity σ_{xy} and diagonal conductivity σ_{xx} vs gate voltage V_{G} in the lowest four Landau levels in a Si(001) MOS inversion layer in a magnetic field $B = 15\,\text{T}$ at temperatures $T = 1.5\,\text{K} \sim 7.7\,\text{K}$.[61]

Ando and Uemura's result of the self-consistent Born approximation.[58] The Hall conductivity σ_{xy} measured by the Hall current method agrees well with the theoretically calculated σ_{xy}.

In the Oji International Seminar held in Hakone in 1980, Kawaji and Wakabayashi[61] presented precise behaviours of the diagonal and Hall conductivities and their temperature dependence observed in a magnetic field 15 T at temperatures between 1.5 K and 7.7 K as shown in Fig. 26. Figure 27 shows the results at 1.5 K which clearly demonstrates the quantized steps in the Hall conductivity for $2e^2/h$ in the Landau gap between the $(0\uparrow -)$ level and the $(0\downarrow +)$ level and for $4e^2/h$ in the Landau gap between the $(0\downarrow -)$ level and the $(1\uparrow +)$ level.[62] (See Fig. 5 for the Landau level index $(n, \uparrow\downarrow \pm)$.)

The quantized Hall conductivity in Fig. 27 demonstrates the characteristic feature of the electron-hole symmetry; i.e., near the spin gap, the Hall conductivity becomes $2e^2/h$ when the Fermi level lies in the localized states in the upper edge of the $(0\uparrow -)$ level even if the $(0\uparrow -)$ level is not completely filled or when the holes in the $(0\uparrow -)$ are localized as well as the case where the electrons in the $(0\downarrow +)$ level are localized or the Fermi level lies in the localized states in the lower edge of the $(0\downarrow +)$ level.

The quantized Hall steps and the electron-hole symmetry in the Anderson localization in Landau

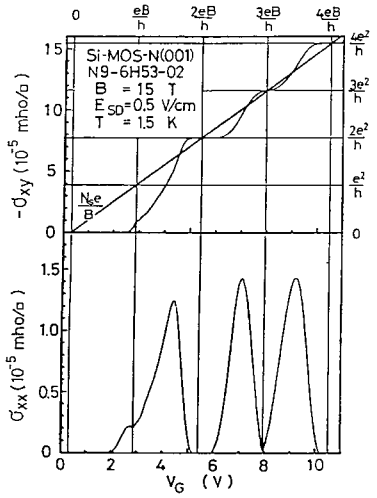

Fig. 27. Hall conductivity σ_{xy} and diagonal conductivity σ_{xx} vs gate voltage V_G in the lowest four Landau levels in a Si(001) MOS inversion layer in 15 T at 1.5 K.[62]

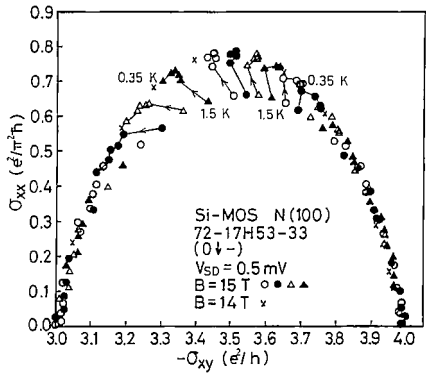

Fig. 28. Diagonal conductivity σ_{xx} versus Hall conductivity σ_{xy} in the $(0\downarrow -)$ Landau level in a Si(001) inversion layer.[68]

levels in 2DES have long been expected by Ando *et al.*'s theory of the Hall effect in 2D systems as shown in Fig. 23. One of the important conclusion reached by Ando *et al.*[53] is their result (3) which is obtained for the case where the impurity bands are separated from the main Landau level. The single-site approximation which Ando *et al.* employed has led the impurity bands separated from the main Landau level. However, the localized states exist actually near the edges of each Landau level instead of the impurity bands. Therefore, it is easy to expect the appearance of the quantized Hall plateaus and the electron-hole symmetry in the localization in Landau levels in 2D systems. Let us imagine a situation where there are many impurity levels separated from each other with very small gaps near the edges of each Landau level and these impurity levels have no electrical conduction.[54] Then we can expect the quantized Hall plateaus and the electron-hole symmetry from Ando *et al.*'s result (3).

4.3. Correlation between diagonal and Hall conductivities of Si(001) MOS inversion layers in strong magnetic fields. In the nonlinear σ model in a theoretical study of localization in 2DES in strong magnetic fields, Levine, Libby and Pruisken[63] assumed that the diagonal conductivity σ_{xx} and the Hall conductivity σ_{xy} are independent scaling variables. Ando and Aoki showed that there is a correlation depending on the Landau quantum number between the diagonal conductivity σ_{xx} and the Hall conductivity σ_{xy}.[64–67]

Yamane, Wakabayashi and Kawaji[68] studied correlation between σ_{xx} and σ_{xy} in Landau levels $(0\downarrow +)$, $(0\downarrow -)$, $(1\uparrow +)$, $(1\uparrow -)$, $(1\downarrow +)$ and $(1\downarrow -)$ in Si(001) MOS inversion layers in magnetic field of 15 T at six temperatures between 1.5 K and 0.35 K. The sample used was an n-channel Si-MOSFET on a (001) surface of a p-type substrate with resistivity of 100 Ω-cm. The peak electron mobility is 14,000 $\mathrm{cm^2/V{\cdot}s}$ at 1.5 K. Measurements were carried out by Hall current method. As an example, $(\sigma_{xx}, -\sigma_{xy})$ plots of the experimental results for the gate voltages in the $(0\downarrow -)$ Landau subband are shown in Fig. 28. The $(\sigma_{xx}, -\sigma_{xy})$ points obtained at three temperatures below 0.87 K in 15 T lie on a single curve. The crosses obtained at 0.35 K in 14 T lie on the same curve. This result demonstrates that the diagonal conductivity correlates with the Hall conductivity at low temperatures. A feature of this figure is that the diagonal conductivity σ_{xx} is symmetrical to the Hall conductivity $-\sigma_{xy}$.

Other $(\sigma_{xx}, -\sigma_{xy})$ plots for $(0\downarrow +)$, $(1\uparrow +)$, $(1\uparrow -)$, $(1\downarrow +)$ and $(1\downarrow -)$ Landau subbands show that there exist correlation between σ_{xx} and σ_{xy}.

Their experimental results are consistent with numerical studies by Ando and Aoki[64–67] which show that the diagonal and the Hall conductivities are not independent scaling variables in Anderson localization in Landau subbands in a 2DES.

4.4. Temperature dependence of Anderson localization in Landau levels: effective mobility edge. Anderson localization in Landau levels or Landau subbands[43] plays very important roles in

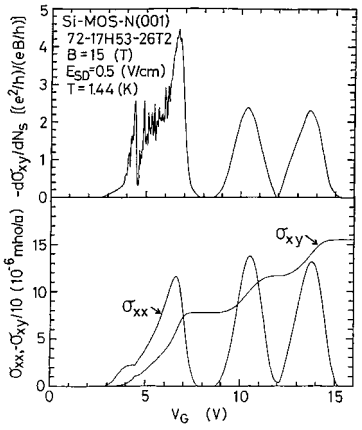

Fig. 29. Diagonal conductivity σ_{xx}, Hall conductivity σ_{xy} and $-d\sigma_{xy}/dN_s$ (N_s electron concentration) against gate voltage V_G in the $N = 0$ Landau levels in a Si(001) inversion layer.[70]

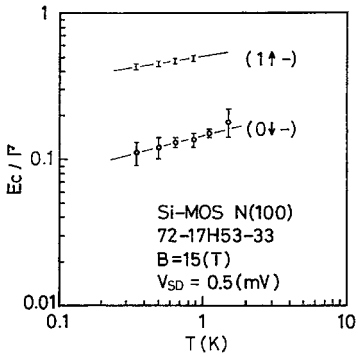

Fig. 30. Temperature dependence of the mobility edge E_c normalized by the broadening Γ in the $(0 \downarrow -)$ and the $(1 \uparrow -)$ Landau subband. Exponent q in $E_c/\Gamma \propto T^q$ is 0.25 and 0.15 in the $(0 \downarrow -)$ and the $(1 \uparrow -)$ Landau subband, respectively.[71]

the quantum Hall effect (QHE) as shown in Fig. 26 and Fig. 27.

Kawaji, Wakabayashi and Moriyama[69] tried to analyze the localization based on a mobility edge model. Moriyama and Kawaji[70] discussed temperature dependence of the mobility edge derived from experimental temperature dependence of $d\sigma_{xy}/dN_s$ or $d\sigma_{xy}/dV_G$. When the localization is so strong that the contribution from the σ_{xx} term to the σ_{xy} is very small, $d\sigma_{xy}/dN_s$ is a useful quantity in the analysis of experimental results. Figure 29 shows σ_{xx}, σ_{xy} and $d\sigma_{xy}/dN_s$ against gate voltage in the $n = 0$ Landau levels in a Si(001) inversion layer.[70]

Wakabayashi, Yamane and Kawaji[71] measured temperature dependence of the Hall conductivity in a Si(001) inversion layer at temperatures 1.5 K, 1.1 K, 0.87 K, 0.65 K, 0.50 K and 0.35 K in a magnetic field $B = 15$ T. They studied localization in $(0 \downarrow -)$ and $(1 \uparrow -)$ Landau subbands. To find the mobility edge E_c refered to the center of the Landau subband by a model calculation which reproduces the experimental line shape of $d\sigma_{xy}/dN_s$ vs N_s at each temperature, they used a density of states given as

$$D(E) = (eB/h)(2/\pi)^{1/2}\Gamma^{-1} exp(-2(E/\Gamma)^2) \qquad [29]$$

where Γ is the broadening of the Landau subband. The change in the Hall conductivity is assumed to be given by

$$\Delta\sigma_{xy}(\nu, T) = -(e^2/h)n_M(\nu, T)/N_M \qquad [30]$$

where ν is the filling factor, n_M is the number of electrons in the delocalized states and N_M is the total number of the delocalized states. They assumed that the density of states and the mobility edges are symmetric with respect to the center of the Landau subband and that the broadening Γ does not change with ν. The temperature dependence of E_c/Γ which reproduces $d(-\sigma_{xy})/dN_s$ for the $(0 \downarrow -)$ Landau subband is plotted on a *log-log* scale in Fig. 30. For the $(1 \uparrow -)$ Landau subband, their simple model cannot reproduce $d(-\sigma_{xy})/dN_s$ as a whole. Therefore, E_c/Γ values which can reproduce the lower shoulder of the $d(-\sigma_{xy})/dN_s$ curve at temperatures below 0.87 K are plotted against T in the figure. When we describe the temperature dependence of E_c/Γ as $E_c/\Gamma \propto T^q$ by the straight lines in Fig. 30, we have $q = 0.25$ for the $(0 \downarrow -)$ Landau subband and $q = 0.15$ for the $(1 \uparrow -)$ Landau subband.

The energy dependence of the inverse localization length $\alpha(E)$ has been studied by Ando,[64] Aoki and Ando[65),67] and Ando and Aoki.[66] Their results show that

$$\alpha(E) \propto |E|^s \qquad [31]$$

where the critical exponent s has been shown to be $s \leq 2$ for the Landau level with the quantum number $n = 0$ and $s \leq 4$ for $n = 1$.

As Aoki and Ando[67] discussed, a cutoff length L_ϵ which destroys the localization in a Landau subband at finite temperatures is given by

$$L_\epsilon \sim (\tau_\epsilon/\tau)^{1/2}\ell_B \qquad [32]$$

where τ_ϵ is the inelastic scattering time, τ the relaxation time related to the broadening Γ by $\Gamma\tau \simeq$

$\hbar$ and ℓ_B the radius of the ground Landau orbit. When we combine Eq. [31] and [32] assuming $\tau_\epsilon \propto T^{-p}$, the temperature dependence of the mobility edge is expected to be

$$E_c/\Gamma \propto T^{p/2s}. \qquad [33]$$

When we use $s = 2$ for the $(0 \downarrow -)$ Landau subband and $s = 4$ for the $(1 \uparrow -)$ Landau subband, the results in Fig. 30, i.e. $q = 0.25$ for the $(0 \downarrow -)$ Landau subband and $q = 0.15$ for the $(1 \uparrow -)$ Landau subband, give us $p = 1.0$ for the former and $p = 1.2$ for the latter.[71]

Results of temperature dependence of τ_ϵ so far studied in weak magnetic fields for Si inversion layers have shown that $p = 1 \sim 1.8$ depending on N_s and T.[46] The present results are in good agreement with these numbers for the exponent p.

5. High precision measurements of quantized Hall resistance and new international electrical reference standard based on QHE

5.1. High precision measurements of quantized Hall resistance by ETL-GU. In 1980, von Klitzing, Dorda and Pepper[72] made a high precision measurement of the quantized Hall resistance $R_H(4) = h/4e^2$ in a Si(001) MOS inversion layer and confirmed the quantization in precision of 3.8 ppm to the recommended values of the fundamental physical constants.

In the same year, Electrotechnical Laboratory (ETL) and Gakushuin University (GU) group carried out high precision measurements of the quantized Hall resistance $R_H(4)$ of Si-MOSFETs. A result of high precision measurements of $R_H(4)$ by Yamanouchi *et al.* (ETL-GU)[73] is shown in Fig. 31. The sample they used is a Hall bar of a Si-MOSFET whose structure is shown in Fig. 6(b). The sample has an oxide thickness of 200 nm, a total length of 600 μm, width of 100 μm and a peak electron mobility of 13,600 $cm^2/V{\cdot}s$. At gate voltages between 14.4 V and 14.6 V, $R_{PP'} = 4\rho_{xx}$ ($L_{PP'} = 400\,\mu m, W = 100\,\mu m$) passes through a minimum ($\simeq 5 \times 10^{-4}$ Ohm) ($\bar{R}_{PP'} \simeq 5 \times 10^{-3}\,\Omega$) and R_H passes a plateau, $R_H = 6453.2024 \pm 0.0008\,\Omega$. We remark here that $\tan\theta_H = \sigma_{xy}/\sigma_{xx} \simeq 5 \times 10^6$ with θ_H being Hall angle. The variation of the filling factor ν of one Landau level corresponding to $\Delta V_G = 14.6\,V - 14.4\,V$ is $\delta\nu(\rho_{xx} \simeq 0) \simeq 6\%$, and the variation of ν for the Hall plateau is much larger than it.

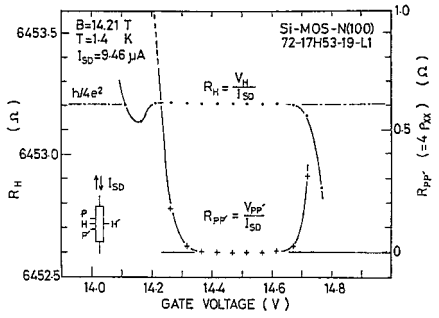

Fig. 31. Results of high precision measurements of quantized Hall resistance $R_H(4)$ and transverse resistance $R_{PP'}$, in the gap between $(0 \downarrow -)$ and $(1 \uparrow +)$ Landau levels in an n-channel Si(001) MOSFET.[62),73]

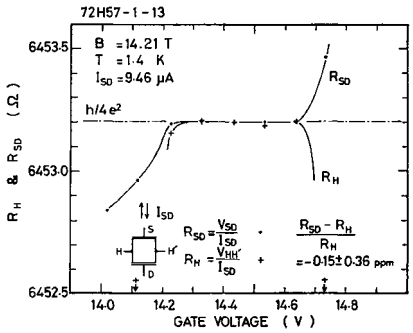

Fig. 32. Quantized Hall resistance $R_H(4)$ and source-to-drain resistance $R_{SD}(4)$, in the gap between $(0 \downarrow +)$ and $(1 \uparrow +)$ Landau levels in an n-channel Si(001) MOSFET.[73]

Yamanouchi *et al.*[73] also reported the results of measurements of source-to-drain resistance $R_{SD} = V_{SD}/I_{SD}$ as well as Hall resistance in a large square Hall bar ($L = W = 1600\,\mu m$) as shown in Fig. 32. In the $n = 4$ case, the average value of R_{SD} and R_H are almost equal, i.e., $(\bar{R}_{SD} - \bar{R}_H)/\bar{R}_H = (-0.15 \pm 0.36)$ ppm, which is within the random uncertainty of measurements. It is remarked here that this result shows clearly the resistance between highly doped electrodes and the 2DES in the inversion layer to be very small. Figure 33 shows a schematic diagram of potential distribution in a long Hall bar in the quantum Hall effect condition.

Yamanouchi reported their results in June 8–12, 1981 in the meeting on Precision Measurements and Fundamental Constants held in National Bureau of Standards (NIST at present) in USA. All the papers presented in the meeting were published in 1984 as given by the reference 73.

Yoshihiro *et al.* (ETL-GU)[74] extended meas-

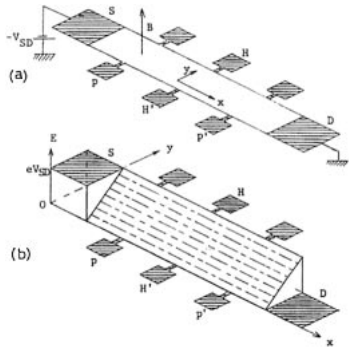

Fig. 33. In a long Hall bar (a) supplied with a voltage V_{SD} between the source electrode S and drain electrode D, electronic energy levels change under the quantized Hall effect condition as shown in (b).[62]

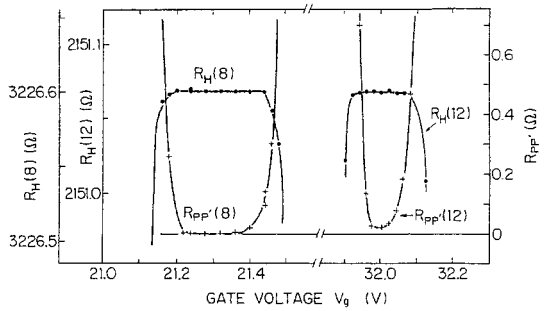

Fig. 34. Hall resiatance and transverse resistance of the Si-MOSFET 72-17H53-17-L1($\mu_{max}(1.3\,\mathrm{K}) \simeq 1.4\times10^4\,\mathrm{cm^2/V{\cdot}s}$) in the gate voltages around the $i=8$ and $i=12$ plateaus. $T\simeq 0.5\,\mathrm{K}$, $B=10.5\,\mathrm{T}$ and $I_{SD}=9.9\,\mu\mathrm{A}$.[74]

urements of quantized Hall resistances to $R_H(8)=h/8e^2$ and $R_H(12)=h/12e^2$ at temperature $T\simeq 0.5\,\mathrm{K}$ in the magnetic fields $B=9.0\,\mathrm{T}$ and $10.5\,\mathrm{T}$. Figure 34 shows the Hall resistance $R_H(i)$ and transverse resistance $R_{PP'}(i)$ plotted against V_G around $i=8$ and $i=12$ in the V_G region around the minimum of $R_{PP'}(i)$. Here $R_H=\rho_{xy}\simeq -1/\sigma_{xy}$ and $R_{PP'}=(\ell/w)\rho_{xx}$ where $\ell/w=4$ for the present sample. It has been found the values of ρ_{xx} at $T\simeq 0.5\,\mathrm{K}$ are about two orders of magnitude smaller than those at $T\simeq 1.3\,\mathrm{K}$. The quantized Hall resistance plateau corresponding to $i=8$ and $i=12$ looks flat within the resolution of measurement, $\simeq 0.001\,\Omega$, in contrast to the previous experiment.

The absolute values of R_H are subject to systematic uncertainties of the unit of $1\,\Omega$ maintained at the ETL. However most of these uncertainties are canceled in the ratio of R_H's when the

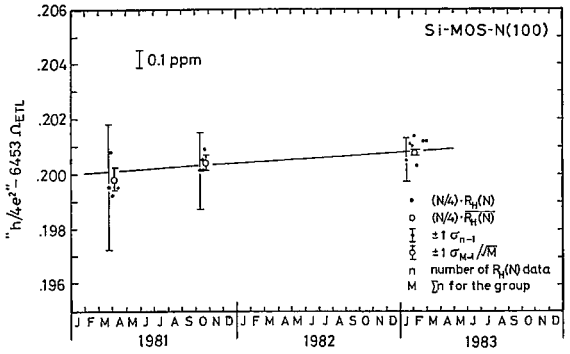

Fig. 35. The "$h/4e^2$" values reffered to $1\,\Omega_{ETL}$. Closed dots: $(N/4)\cdot R_H(N)$ values; open circles: average values $(N/4)\cdot \bar{R}_H(N)$ each taken over the group of measurements it belongs to; vertical bars with the closed dots: typical $\pm 1\sigma_{n-1}$ for each set of measurements; vertical bars with the open circles: $\pm 1\sigma_{M-1}/\sqrt{M}$ for each group of measurements. Here, n is the number of $R_H(N)$ data and $M=\Sigma n$ for the group.[62]

measurements are made on the same sample. A possible change in the unit of quantization is thus detectable to the precision nearly limited by the resolution of measurement. The ratios with their 1σ uncertainties are given as

$$2\times \bar{R}_H(8)/\bar{R}_H(4) = 0.99999993 \pm 0.00000018,$$
$$2\times \bar{R}_H(8)_{9T}/\bar{R}_H(4) = 1.00000005 \pm 0.00000019,$$
$$3\times \bar{R}_H(12)/\bar{R}_H(4) = 0.99999994 \pm 0.00000024.$$

Here $\bar{R}_H(8)_{9\,\mathrm{T}}$ is the mean value of $R_H(8)$ measured at $B=9\,\mathrm{T}$, and the uncertainties include the estimated systematic uncertainty of ± 0.15 ppm. An important result of Yoshihiro *et al.* (ETL-GU) is that the unit of quantization of $-\sigma_{xy}$ is thus experimentally verified to be constant to within the accuracy of present measurement independently of the quantum number or the concentration of electrons in the inversion layer, that implies, independently of the change in scattering properties, interaction between carriers, and number and character of localized states.[74]

After a series of measurements taken over two years, Kinoshita *et al.*[75] found an interesting result as shown in Fig. 35. The figure shows an apparent drift of "$h/4e^2$" value during the period. This is to be interpreted as a drift, which is about $-0.06\,\mu\Omega$ a year, in the magnitude of the as maintained unit Ω_{ETL} (one standard Ohm in the SI system maintained in the Electrotechnical Laboratory).

5.2. High precision measurements of quantized Hall resistance by CSIRO-GU-ETL. On

the basis of extensive investigation of the quantum Hall effect by GU[60)–62)] and ETL-GU,[73)–76)] we constructed a new measurement system of the QHE in GU including a 15.6 T superconducting magnet, a voltage comparator system using a Guildline 9930 DCC potentiometer, and a cryogenic current comparator (CCC) resistance bridge,[77)] supported by a Grant-in-Aid for Specially Promoted Research, Ministry of Education, Science and Culture (1985–1988). We used the new measurement system for determination of the value of the $R_{\rm H}(4)$ for Si-MOSFETs in terms of the realization of the SI ohm at the National Measurement Laboratory (NML) of the Commonwealth Scientific and Industrial Research Organization (CSIRO) in Australia.[78),79)] Experimental equipment and procedure are given in detail by Kawaji *et al.*[80)]

Three 1-Ω standard resistors and the 83 elements build-up resistor (BUR) were hand carried by Brian W. Ricketts from CSIRO to GU on March 7, 1988 and returned on April 6, 1988. Determination of the values of reference resistors $R_{\rm R}(4)$ whose nominal values are 6453.2 Ω were made in two ways: (1) via the 83 element BUR from March 17–April 2, 1988, and (2) via the CCC resistance bridge using a step-up sequence of 1–10 Ω, 10–100 Ω and 100–6453.2 Ω($R_{\rm R}(4)$). We made measurements of the quantized Hall resistance $R_{\rm H}(4)$ for Si-MOSFETs on March 29, May 10 and May 14, 1988, by comparing $R_{\rm H}(4)$ to a reference resistor $R_{\rm R}(4)$. The final result could be expressed as $R_{\rm H}(4) = 6453.20\ \ 336(52))\Omega_{\rm SI\text{-}NML}$ or $R_{\rm H}(4) = 6453.2(1.000\ \ 000\ \ 52(8))\Omega_{\rm SI\text{-}NML}$. The result[80)] was reported to B.N. Taylor (NIST) and T.J. Witt (BIPM) in the Working Group on the Quantum Hall Effect.

5.3. New international electrical reference standard $R_{\rm K\text{-}90}$ based on the quantum Hall effect. Taylor and Witt[81)] presented the background and basis for the new international electrical reference standards of voltage and resistance that were to come into worldwide use starting on the 1 January 1990. They described that founded on the Josephson and quantum Hall effects, respectively. These new reference standards for voltage and resistance have improved significantly the international uniformity of electrical measurements and their consistency with the SI. Taylor and Witt were serving as coordinators of the Working Group on the Josephson Effect and the Working Group on the Quantum Hall Effect in the Comité Consultatif d'Électricité (CCE). Figure 36 was included in the report of Taylor and Witt to CCE in October 1988. Our measurement result of $R_{\rm K} = i \times R_{\rm H}(i)$ value is shown as CSIRO/GU in the Fig. 36. The term CSIRO/GU means that the quantized Hall resistance was measured in GU based on the SI ohm by CSIRO calculable capacitor. The value of von Klitzing constant, now called as $R_{\rm K\text{-}90}$, recommended by Taylor and Witt based mainly on the $R_{\rm K}$ values measured by NIST (USA), NPL (UK) and CSIRO (Australia) and assigned uncertainty σ are given by

$$R_{\rm K\text{-}90} = (25\ 812.807 \pm 0.005)\,\Omega. \qquad [34]$$

The relative standard deviation uncertainty is 2×10^{-7}.

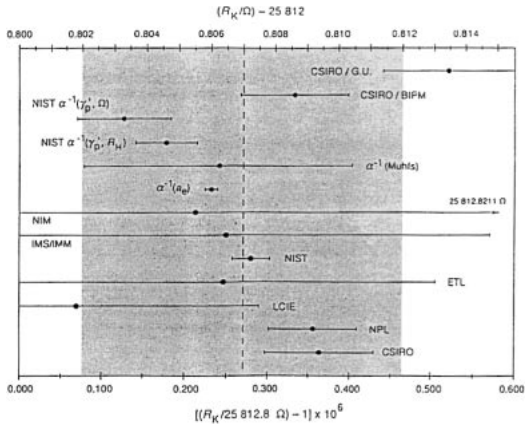

Fig. 36. Comparison of the recommended value of $R_{\rm K}$ (the middle vertical line) and its assigned standard deviation uncertainty (deliminated by the shading) with the values of $R_{\rm K}$ and their standard deviation uncertainties as reported from the researchers in the laboratories.[81)]

The relative standard deviation uncertainty is 2×10^{-7}.

5.4. Reconstruction of the high precision measurement system in GU and results in GaAs/AlGaAs heterostructures by CSIRO/GU. An important result shown in Fig. 36 is a significant difference between the $R_{\rm K}$ values measured by CSIRO and CSIRO/GU. The $R_{\rm K}$ value by CSIRO/BIPM is in good agreement with the CSIRO value. The result shows that the measurement system or the Hall device in GU has unknown defects. Nagashima *et al.* (GU-ETL)[82)] made measurements of $R_{\rm H}(4)$ and $R_{\rm H}(2)$ of a GaAs/AlGaAs heterostructure Hall device against the reference resistors $R_{\rm R}(4)$ and $R_{\rm R}(2)$ whose values are close to $h/4e^2$ and $h/2e^2$.

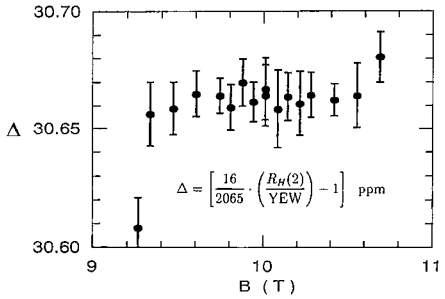

Fig. 37. Results of comparisons of the QHR $R_{\rm H}(2)$ in the $i = 2$ Hall plateau against a 100 Ω standard resistor called YEW by a cryogenic current comparator (CCC) bridge carried out by Nagata in December 1992 in GU. The current in the GaAs/AlGaAs Hall device was 35 μA.[83]

The values of $R_{\rm R}(4)$ and $R_{\rm R}(2)$ were compared with a 100 Ω standard resistor via a CCC resistance bridge. Results showed that $(4 \times R_{\rm H}(4) - 2 \times R_{\rm H}(2))/2 \times R_{\rm H}(2) = (0.037 \pm 0.019) \times 10^{-6}$. The result shows an unknown defect in the measurement system.

We started to reconstruct the high precision measurement system in the spring of 1990.[83] Greig W. Small and Brian W. Ricketts from CSIRO helped us.

Our high precision measurement system consists of two systems. One is a voltage comparator (VC) system using a Guildline 9930 potentiometer and the other is a cryogenic current comparator (CCC) bridge system. The manually operated VC system was reconstructed into an automatically operated VC system by Nagata.[83] Electronic circuits in the CCC system were also reconstructed. In December 1990, Greig Small visited GU from CSIRO, and advised us on the reconstruction of the measurement system. We started new measuements of QHR in January 1992 on a GaAs/AlGaAs heterostructure Hall device. W. Schwitz (OFM) provided a GaAs/AlGaAs device EPF234/7 for GU.

Figure 37 shows results of comparisons of the QHR $R_{\rm H}(2)$ in the $i = 2$ Hall plateau against a 100 Ω standard resistor called YEW by a cryogenic current comparator (CCC) bridge carried out by Nagata[83] in December 1992 in GU.

In Fig. 38, five $R_{\rm K}$ values below the dotted horizontal line are measured in GU based on the SI ohm by CSIRO between March 1992 and September 1994.[84] They are in good agreement with the $R_{\rm K}$ value reported by CSIRO in 1988 shown in Fig. 36.

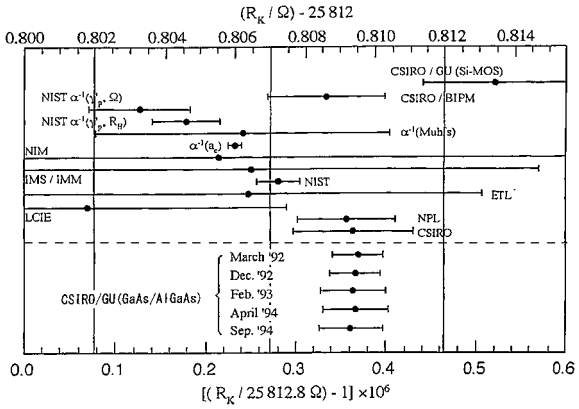

Fig. 38. Five $R_{\rm K}$ values below the dotted horizontal line are measured in GU based on the SI ohm by CSIRO between March 1992 and September 1994.[84] The measurements of March '92 and Dec. '92 were carried out by Nagata and measurements of Feb. '93, April '94 and Sep. '94 were carried out by Hayashi. They are in good agreement with the $R_{\rm K}$ value reported by CSIRO in 1988 in Fig. 36. The part above the horizontal dotted line are results included in Fig. 36.

6. Fractional quantum Hall effect: activation energies in 1/3 and 2/3 FQHE

Since the first observation by Tsui, Stormer and Gossard[85] and Tsui *et al.*[86] in 2DES of GaAs/$Al_{0.3}Ga_{0.7}As$ heterostructures, the fractional quantum Hall effect (FQHE) has attracted much interest both experimentally and theoretically. The phenomenon is characterized by formation of the plateaus in the Hall resistivity ρ_{xy} and concurrent vanishing of the diagonal resistivity ρ_{xx} similar to integer quantum Hall effect except that the filling factor becomes a fractional number $\nu = p/q$; $p = 1, 2, 3 \ldots$ and $q = 3, 5, 7 \ldots$. The filling factor ν is defined by $\nu = N_{\rm s}h/eB$, where $N_{\rm s}$ is electron number density and eB/h is the degeneracy of a Landau level. In particular, the 1/3 and 2/3 effects appear more prominently than other fractional effects. Theoretical studies[87)–93)] have shown that the phenomenon is associated with the formation of a new liquid-like condensed electronic state arising from the strong electron-electron Coulomb interaction.

Chang *et al.*[94] measured temperature dependence of ρ_{xx} near the 2/3 FQHE in very high mobility samples. They can vary electron density continuously between 1 and $2.1 \times 10^{11}\,{\rm cm}^{-2}$ using a backside gate. The highest mobility achieved is 1.5×10^6 $\rm cm^2/V{\cdot}s$. The temperature dependence show a

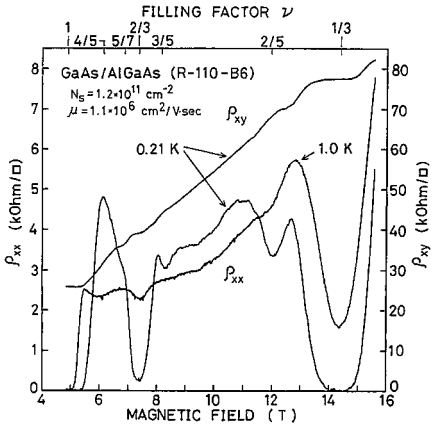

Fig. 39. Magnetic field dependence of the diagonal resistivity ρ_{xx} at $T = 0.21$ and 1.0 K and the Hall resistivity ρ_{xy} at 0.21 K in a GaAs/Al_xGa_{1-x}As heterostructure with very high electron mobility. In addition to the 1/3 and 2/3 effect, 2/5, 3/5, 4/5 and 5/7 effect are also observed. The upper scale of filling factor is for the help of sight.[95)]

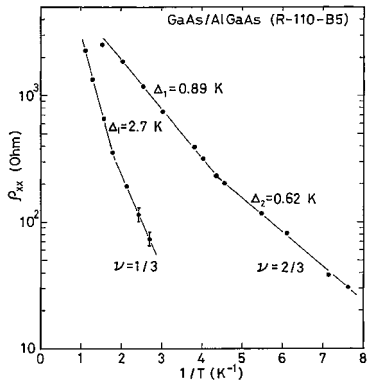

Fig. 40. Temperature dependence of ρ_{xx} minima at $\nu \simeq 1/3$ ($B = 14.6$ T) and $\nu \simeq 2/3$ ($B = 7.4$ T) where ν is the filling factor of a Landau level.[95)]

single straight line for each ν ($0.6 \leq \nu \leq 0.665$) in $log\rho_{xx}$ vs $1/T$ plots between 0.4 K and 0.065 K. The activation energy at $\nu = 2/3$ is $\Delta(2/3) = 0.830$ K.

Kawaji, Wakabayashi, Yoshino and Sakaki measured activation energies of ρ_{xx} around $\nu = 1/3$ and 2/3 in very high mobility samples by varying magnetic fields up to 15.5 T at temperatures down to 0.1 K.[95)] The samples used are modulation doped GaAs/Al_xGa_{1-x}As($x \simeq 0.3$) heterostructures grown by molecular beam epitaxy. The layer structure consists of 1.2 μm undoped GaAs, 500 A of undoped AlGaAs, 1500 A Si-doped (2×10^{17} cm^{-3}) AlGaAs, and 100 A of undoped GaAs. Surface electron density and electron mobility at 1 K are $N_s = 1.2 \times 10^{11}$ cm^{-2} and $\mu = 1.1 \times 10^6$ cm^2/V·s, respectively. The total length of the samples, the potential probe distance and the width are 600 μm, 200 μm and 50 μm, respectively.

Behavior of the magnetic field dependence of ρ_{xy} and ρ_{xx} is shown in Fig. 39. In addition to the 1/3 and 2/3 FQHE, clear minima are observed at $\nu = 2/5$ and 3/5 in ρ_{xx} at 0.21 K and at $\nu = 4/5$ in ρ_{xx} at 1.0 K. Clear shoulders are also observed at $\nu = 5/7$ in both ρ_{xx} and ρ_{xy} at 0.21 K. Two samples showed nearly the same behavior.

Figure 40 shows temperature dependence of ρ_{xx} at $\nu \simeq 1/3$ and $\nu \simeq 2/3$ at fixed magnetic fields of 7.4 T and 14.6 T. Each line of $log\rho_{xx}$ vs $1/T$ plots at $\nu \simeq 1/3$ and $\nu \simeq 2/3$ in Fig. 40 consists of two straight lines. The sharp break in the temperature dependence looks to show that the mechanism of electron transport changes at these temperetures. We determined activation energies Δ_1 and Δ_2 by $\rho_{xx} \propto \exp(-\Delta/T)$ in the high and the low temperature regions, respectively. Two samples have similar temperature dependence characterized by Δ_1 and Δ_2.

We describe the creation energy of the quasi particles as

$$\Delta_{q.p} = \frac{C_{q.p}e^2}{\kappa \ell_B} \qquad [35]$$

where $C_{q.p}$ is a numerical constant, κ dielectric constant, and $\ell_B = \sqrt{\hbar/eB}$ magnetic length. After Laughlin,[88),90)] $C_{q.e} = 0.030$, $C_{q.h} = 0.026$. Chacraborty derived $C_{q.e} = 0.025$.[91)] Haldane and Rezayi[92)] derived for a pair creation $C_{q.e} + C_{q.h} = 0.105$.

When we follow Laughlin,[88),90)] We have $\Delta q.e. = 5.8$ K and $\Delta q.h. = 5.0$ K at $B = 14.6$ T. As Yoshioka[93)] discussed, these values suffer reduction of about 50% by the three dimensionality and about 10% by the mixing of higher Landau levels. The experimental result $\Delta_1(1/3) = 2.7$ K is in good agreement with the theoretical results.

In the case of $\nu = 2/3$, electron-hole symmetry requires that the ratio of $\Delta(1/3)$ and $\Delta(2/3)$ for the same sample is $\sqrt{2}$ as activation energy is scaled by $e^2/\kappa\ell_B$. However experimental results show that $\Delta(1/3)/\Delta(2/3) \simeq 3$. This discrepancy cannot be understood.

Further experimental studies for activation energies of the 1/3 and 2/3 FQHE have been made by Wakabayashi, Kawaji, Yoshino and Sakaki,[96),97)] and by Wakabayashi, Sudou, Kawaji, Hirakawa

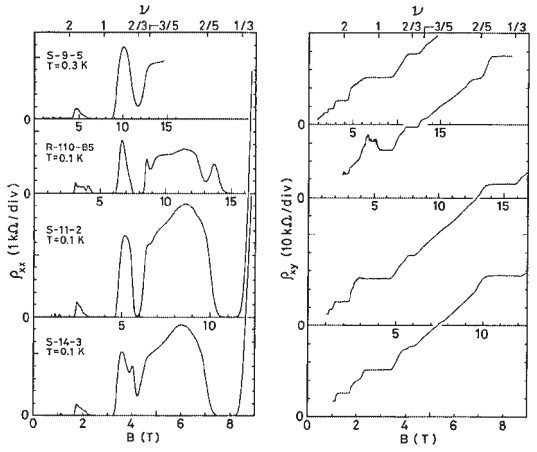

Fig. 41. (a) Magnetic field dependences of the diagonal resistivity ρ_{xx} in four GaAs/Al_xGa_{1-x}As heterostructures. The current used is 10 nA (2×10^{-6} A/m). The magnetic field is normalized at the filling factor $\nu = 2/3$. (b) Magnetic field dependendes of the Hall resistivity corresponding to (a). The ρ_{xy} larger than h/e^2 for $\nu \geq 1$ of the sample R-110-B5 is probably due to a contact effect.[96)]

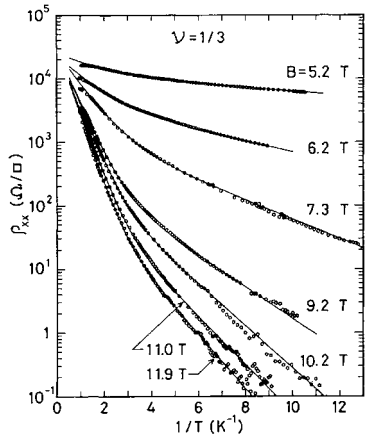

Fig. 42. Temperature dependence of the diagonal resistivity minima at $\nu \simeq 1/3$ for each gate bias between −50(top) and +167 V(bottom) in sample A. The current used is 5 nA except for 5.2 T (2 nA) and 7.3 T (10 nA). Each solid line represents a fitted curve for Eq. [36].[101)]

and Sakaki[98)–101)] for various samples.

Figure 41 shows typical traces of ρ_{xx} and ρ_{xy} against the magnetic field B for each class of samples. The magnetic field is normalized at $\nu = 2/3$. In addition to the 1/3 and 2/3 effects, clear minima of ρ_{xx} and clear shoulders in ρ_{xy} are observed at $\nu = 2/5$ and 3/5 and also minima of ρ_{xx} at $\nu = 4/3$ and 5/3 are observed in the sample R-110-B5. The Hall resistivity ρ_{xy} larger than h/e^2 for $\nu \geq 1$ of this sample is probably due to a contact effect.

Figure 42 shows an example of experimental results of temperature dependence of the resistivity in $\nu = 1/3$ FQHE in a GaAs/$Al_{0.3}Ga_{0.7}$As heterostructure called sample A measured at temperatures between 1.2 K and 70 mK. The electron concentration N_s and the electron mobility μ were controlled between 4.3×10^{14} and 9.7×10^{14} m^{-2}, and 14 and 62 m^2/V·s, respectively, by applying a bias voltage between −50 and 167 V on the backside gate.[101)] Each solid line represents a fitted curve for the equation

$$\rho_{xx}(T) = \rho_{01} e^{-W_1/T} + \rho_{02} e^{-W_2/T} \qquad [36]$$

where W_1 represents the activation energy measured in kelvin in the high temperature region and W_2 in the low temperature region, respectively.

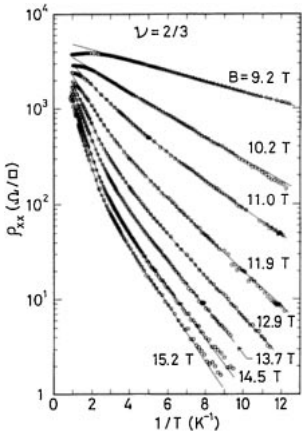

Fig. 43. Temperature dependence of the diagonal resistivity minima at $\nu \simeq 2/3$ for each gate bias between −58 V(top) and +68 V(bottom) in sample B. The current used is 0.2 nA for the field between 9.2 T and 11.9 T, and 2.0 nA between 12.9 T and 15.2 T. Each solid line represents a fitted curve for Eq. [36].[98)]

They studied the 2/3 effect by use of sample B whose electron concentration and electron mobility were controlled between 1.5×10^{15} and 2.5×10^{15} m^{-2}, and 27 and 88 m^2/V·s, respectively.[98)]

Magnetic field dependence of the activation energy W_1 for $\nu = 1/3$ FQHE in the sample A and $\nu = 2/3$ FQHE in the sample B are shown in Fig. 44. This figure contains all W_1 data so far measured by Wakabayashi *et al.*[96)–98),101)] connected by broken lines. (Closed symbols are data for $\nu =$

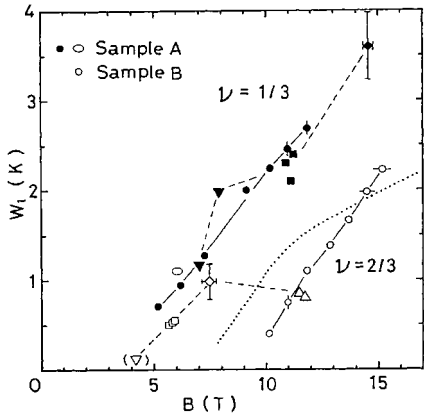

Fig. 44. Magnetic field dependence of the activation energy W_1. Closed symbols are data for $\nu = 1/3$ and open symbols for $\nu = 2/3$. The dotted line shows results from references 94 and 102. The broken lines connect the data taken from samples with no backside gate.[96),101)] Properties of samples as shown by the symbol of the sample follows (N_s in $10^{14}\,\mathrm{m}^{-2}$ and μ in $\mathrm{m}^2/\mathrm{V{\cdot}s}$). ◇ and ◆ (12 and 110), ■ (9.4 and 21), ▼ (6.8 and 28) and (5.6 and 23), △ (190 and 32), ▽ (68 and 28).[96)] Sample A (4.3∼9.7 and 14∼62).[101)] Sample B (15∼25 and 27∼88).[98)]

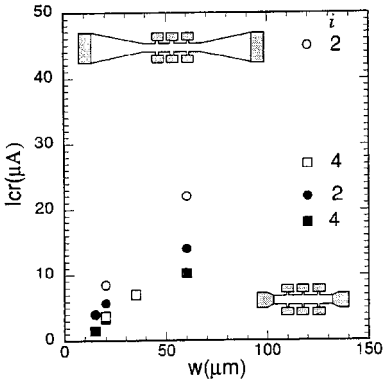

Fig. 45. Critical current of the breakdown I_{cr} versus sample width w in butterfly Type I Hall bars (open symbols) and rectangular Hall bars (full symbols). A butterfly-type Hall bar is schematically shown in the upper left and a rectangular Hall bar is schematically shown in the lower right.[107)]

1/3 and open symbols for $\nu = 2/3$.) Results by Chang *et al.*[94)] and Boebinger *et al.*[102)] are also shown by a dotted line.

Activation energy in the 1/3 and the 2/3 FQHE is expected theoretically to be expressed by $W_1 = \alpha e^2/\kappa\ell_\mathrm{B}$ which is proportional to $B^{1/2}$. In Fig. 44, $W_1(1/3)$ data make a group but they are not proportional to $B^{1/2}$. $W_1(2/3)$ data are scattered and look to be separated into two groups. One group of $W_1(2/3)$ data at $B \leq 7.5\,\mathrm{T}$ is close to the $W_1(1/3)$ data but another group of $W_1(2/3)$ data at $B \geq 10\,\mathrm{T}$ is much lower than the $W_1(1/3)$ data. Further experimental studies are needed to solve the problem.

7. Breakdown of quantum Hall effect and collapse of quantized Hall resistance at high currents

7.1. Breakdown of quantum Hall effect at high currents. The quantum Hall effect (QHE) appears in a Hall bar as the Hall resistance is quantized as $R_\mathrm{H}(i) = h/ie^2$ (i: an integer) with zero diagonal resistance $R_{xx} = 0$. Breakdown of the QHE appears as an abrupt appearance of R_{xx} in a Hall bar at a high current.[103),104)]

In the QHE, a non-dissipative state appears near the central part of a Hall bar. Joule heat is always generated at both ends of the Hall bar, i.e. in transition regions between the 2DES and two current electrodes.[62)] The breakdown of the QHE which the GU group aimed to measure is appearance of dissipation in a part of a Hall bar other than the parts near the current electrodes. In a series of experiments we used specially designed Hall bars which we call butterfly-type Hall bars fabricated from $\mathrm{GaAs/Al_{0.3}Ga_{0.7}As}$ heterostructure wafers by photolithography and wet chemical etching. Electrode structures, called the butterfly-type I, have the same source and drain electrode width of $W = 400\,\mu\mathrm{m}$ and a large length between the source and the drain electrodes of $L = 2900\,\mu\mathrm{m}$. The length of the central part ℓ is 600 μm long and has a different width w between 10 and 120 μm. The length $\ell = 600\,\mu\mathrm{m}$ is found in three pairs of potential probes. The width of each Hall bar is linearly narrowed from both current electrodes to the ends of the central part as shown in Fig. 45 (See also Fig. 1 in the reference 105). Another type of Hall bars (butterfly Type II) have $W = 400\,\mu\mathrm{m}$, $L = 2600$ μm.[106)] We fabricated the central part of the Hall bar with $\ell = 120\,\mu\mathrm{m} + 12w$ where ℓ and w are length and width, respectively, of the central part. The width of the central part is fabricated as $w = 3$, 4, 5, 10, 20, 50 and 60 μm. The length ℓ is distributed in three pairs of potential probes similar to the Type I.

We compared breakdown features between the butterfly Type I Hall bars and conventional rectangular Hall bars ($L = 600\,\mu\mathrm{m}$) fabricated from the same heterostructure wafer which has $N_\mathrm{s} =$

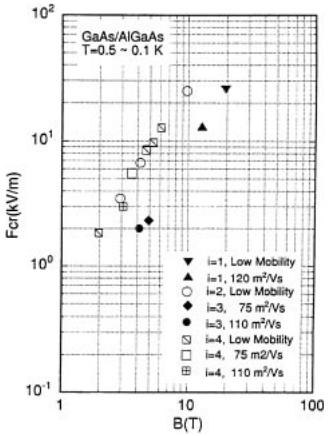

Fig. 46. Critical breakdown Hall electric field $F_{\rm cr}$ versus magnetic field B in butterfly-type Hall bars.[107] Low mobility: $13.5 \le \mu(\mathrm{m^2\,V^{-1}\,s^{-1}}) \le 27$.

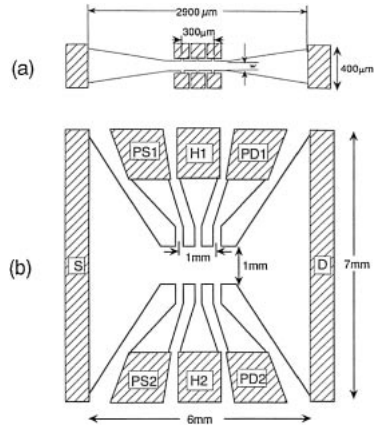

Fig. 47. Hall bars used in the first experiment of the collapse of the QHR. (a) Standard butterfly-type Hall bars. The width $w = 15\,\mu\mathrm{m}$ in the sample LC7 and $w = 35\,\mu\mathrm{m}$ in the sample LC5. (b) Giant butterfly-type Hall bar.[109]

$1.6 \times 10^{15}\,\mathrm{m^{-2}}$ and $\mu = 35\,\mathrm{m^2\,V^{-1}\,s^{-1}}$. An example of the width dependence of the critical breakdown current is shown in Fig. 45.[107] The conventional rectangular Hall bars show a sublinear dependence of $I_{\rm cr}$ on w, while the butterfly Type I Hall bars show a linear dependence. We have extended breakdown measurements for butterfly Type I and butterfly Type II Hall bars fabricated from various wafers. Experimental results for critical breakdown electric field $F_{\rm cr}$ at the center of each Hall plateau with the plateau quantum numbers $i = 1, 2, 3, 4$ are plotted against the magnetic field at the center of each plateau in Fig. 46.[107] Figure 46 shows that $F_{\rm cr}$ $(i = 2, 4)$ lie on a single straight line and $F_{\rm cr}$ $(i = 1, 3)$ lie on another parallel single straight line in the *log-log* plot and their slopes are 3/2.

The magnetic field dependence of the breakdown critical electric field, $F_{\rm cr} \propto B^{3/2}$, is an important fact to find a mechanism for the breakdown. Another important result in Fig. 46 is that the critical breakdown Hall electric field is independent of the electron mobility. Eaves and Sheard[108] have derived a simple expression for the critical breakdown electric field $F_{\rm cr}(\mathrm{E-S}) \propto B^{3/2}$ based on the inter-Landau level tunneling of electrons as the Landau level splitting is proportional to B and the spacial extent of its wave function is inversely proportional to $\sqrt{B}$. However, the magnitude of $F_{\rm cr}(\mathrm{E-S})$ is more than one order of magnitude larger than our experimental results. According to Eaves and Sheard, $F_{\rm cr}(\mathrm{E-S})_{i=2}/F_{\rm cr}(\mathrm{E-S})_{i=4} = 1.5$, while they are the same in our experimental results. Probably a higher order tunneling process should be taken into account to understand experimental results.

7.2. Collapse of quantized Hall resistance at high currents. We refer to the abrupt appearance of deviation of Hall resistance $\Delta R_{\rm H}(i)$ from the quantized value as collapse of the quantized Hall resistance. The phenomena which occur in the QHE at high current have been known since the early 1980s. Most of the research has been carried out, however, on the breakdown of the QHE. Almost no experimental research has been carried out on collapse of the QHR in high precision except Cage *et al.*[104] Since 1998, we have run experiments on collapse of the QHR using "butterfly-type" Hall bars.

In our first experiment on the collapse of the QHR,[109] we fabricated a giant butterfly-type Hall bar (GBH) as shown in Fig. 47(b), as a reference Hall bar from a heterostructure wafer whose electron concentration and mobility at 1 K are $N_{\rm s} = 2.6 \times 10^{15}\,\mathrm{m^{-2}}$ and $\mu = 100\,\mathrm{m^2/V{\cdot}s}$. The GBH has wide current electrodes $(W = 7\,\mathrm{mm})$, with a large distance between them $(L = 6\,\mathrm{mm})$ and a wide central rectangular measurement part with $w = 1\,\mathrm{mm}$ and $l = 2\,\mathrm{mm}$. We also fabricated two standard butterfly-type Hall bars (SBH) with narrow width of the central part $w = 35\,\mu\mathrm{m}$ (SBH-LC5) and $w = 15\,\mu\mathrm{m}$ (SBH-LC7) from a heterostructure wafer whose electron concentration and mobility at 1 K are $N_{\rm s} = 5.3 \times 10^{15}\,\mathrm{m^{-2}}$ and $\mu = 20\,\mathrm{m^2/V{\cdot}s}$.

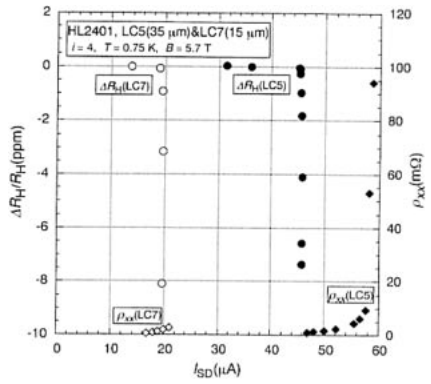

Fig. 48. Deviation of Hall resistance $\Delta R_{\rm H}/R_{\rm H}$ from the quantized value $R_{\rm H}(4) = {\rm h}/4e^2$ and change in diagonal resistivity ρ_{xx} in standard butterfly-type Hall bars SBH-LC5 ($w = 35\,\mu$m) and SBH-LC7 ($w = 15\,\mu$m) against source-drain current $I_{\rm SD}$.[109)]

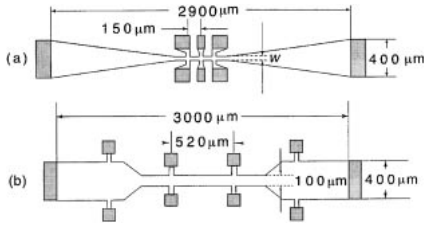

Fig. 49. Electrode structures of Hall bars. (a) Butterfly-type Hall bar with the channel width $w = 15$ or $35\,\mu$m and the voltage probe width $w_{\rm p} = 40\,\mu$m. (b) Jeanneret-type Hall bar with the channel width $w = 100\,\mu$m and the voltage probe width $w_{\rm p} = 50\,\mu$m.[112)]

Quantized Hall resistance $R_{\rm H}(4)$ in the SBH samples and $R_{\rm H}(2)/2$ in the GBH sample were compared directly, using a cryogenic current comparator (CCC) bridge[77),82)] by comparing $I_{\rm SD}$ of each sample for the equal Hall voltages of two samples as $(V_{\rm H1} - V_{\rm H2})_{\rm SBH} = (V_{\rm H1} - V_{\rm H2})_{\rm GBH}$. At low currents, agreement between $R_{\rm H}(4)$ in the SBH samples and $R_{\rm H}(2)/2$ in the GBH sample is within 0.02 ppm. We confirmed that the critical current of breakdown $I_{\rm cr}$ in the GBH sample is about 30 times that of $I_{\rm cr}$ in the SBH-LC5 ($w = 35\,\mu$m) and about 60 times that of $I_{\rm cr}$ in the SBH-LC7 ($w = 15\,\mu$m). Measurements were carried out at $T = 0.75\,$K immersing a SBH sample and the GBH sample into liquid ^{3}He in a magnetic field up to 9 T.

Experimental results are shown in Fig. 48. Each sample shows a sharp decrease in the Hall resistance $R_{\rm H}$ against $I_{\rm SD}$, i.e. collapse of the QHR, at $I_{\rm SD} \sim 19\,\mu$A in the SBH-LC7 and at $I_{\rm SD} \sim 45\,\mu$A in the SBH-LC5 sample, respectively. When we plotted $\Delta R_{\rm H}/R_{\rm H}(4)$ against the Hall electric field $F_{\rm H}$, we found that the collapse of the QHR in these two samples occurs at the same Hall electric field. The finding that a sharp decrease in $R_{\rm H}$ at that value of $I_{\rm SD}$ at which only a gradual change appears in ρ_{xx} is not in agreement with that reported by Cage *et al.*[104)] They reported that the value of $R_{\rm H}$ decreases only by $(0.1 \sim 0.6)$ ppm while R_{xx} shows changes by 6 orders of magnitude during a change of $I_{\rm SD}$ from 25 μA to 370 μA in a rectangular Hall bar which is 4.6 mm long and 0.38 mm wide.

Kawaji, Iizuka, Kuga and Okamoto[110)] confirmed that results of the collapse of the QHR observed using three different pairs of Hall probes shown in Fig. 47(a) are the same, and behaviour of R_{xx} against $I_{\rm SD}$ measured using different pairs of voltage probes along the opposite sides of the Hall bar are also the same.

In order to explain the collapse of QHR and behavior of R_{xx} against Hall electric field $F_{\rm H}$, Kawaji *et al.* proposed a phenomenological model for the electronic structure of a Hall bar in the quantum Hall state.[110)]

We have used a butterfly-type Hall bar in order to escape from effect of electron heating by high electric fields at opposite corners of source- and drain-electrode on a central measurement part of the Hall bar. Jeanneret *et al.*[111)] have used Hall bars which have an electrode structure similar to our butterfly-type Hall bars in their experiment to confirm that $R_{\rm H}(i)$ is independent of device width within the uncertainty $\pm 1 \times 10^{-9}$. As shown in Fig. 49, the following are differences of the electrode structures between the butterfly-type Hall bar and the Jeanneret-type Hall bar: (1) the width w of the channel for measurement, (2) the ratio of the probe width w_p to channel width w, and (3) the distance d_p between adjacent voltage probes along the same side of the measurement channel.

Kawashima, Tanaka and Kawaji[112)] used a Jeanneret-type Hall bar with $w = 100\,\mu$m, $d_p = 520\,\mu$m and $w_p = 50\,\mu$m. Measurements of Hall resistance were made using a cryogenic current comparator (CCC) bridge. In the comparison measurements, 6.45 and 12.9 kΩ metal wire resistor were used for $R_{\rm H}(4)$ measurements. Measurement of $R_{\rm H}$ and ρ_{xx} was made at 1.8 K. Behavior of collapse of the QHR and change in ρ_{xx} with the increase in $I_{\rm SD}$ were measured near the center of the $i = 4$

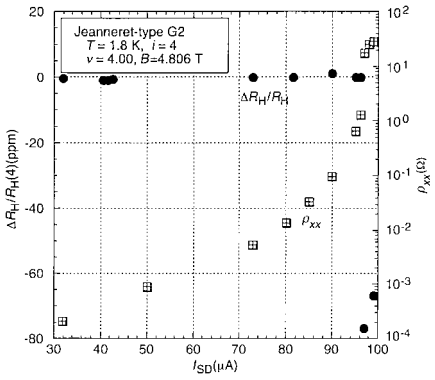

Fig. 50. Collapse of the QHR and breakdown of ρ_{xx} at the center of the $i = 4$ Hall plateau ($\nu = 4$) in a Jeanneret-type Hall bar.[112]

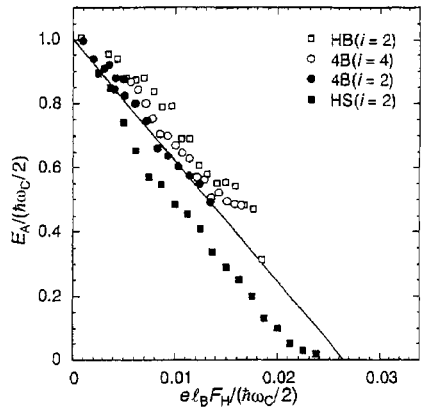

Fig. 51. Hall electric field dependence of the activation energy in the temperature dependence of the diagonal resistivity. The activation energy $E_{\rm A}$ is normalized by $\hbar\omega_{\rm c}/2$ and the Hall electric field $F_{\rm H}$ is normalized by $(\hbar\omega_{\rm c}/2el_{\rm B})$. In sample names such as HB, 4B and HS, "H" and "4" mean wafer's code. B and S means butterfly-type Hall bar and a short channel Hall bar, respectively. The short channel is a 7 μm long(l') and 20 μm wide(w') channel which is made in the central part of a butterfly-type Hall bar.[115]

plateau. As an example, results at $\nu = 4.00$ are shown in Fig. 50. In these experiments, collapse of the QHR and breakdown of non-dissipative state appear at almost the same source-drain current $I_{\rm SD}$.

Significant differences are observed between Jeanneret-type Hall bars and butterfly-type Hall bars. First, in the Jeanneret-type Hall bar, ρ_{xx} increases rapidly with the increase in $I_{\rm SD}$ in a region $I_{\rm SD} > 70\,\mu$A as shown in Fig. 50. Second, collapse of the QHR appears at nearly the same current for the breakdown of the non-dissipative state in Jeanneret-type Hall bars wheras breakdown of non-dissipative state appears at about 1.2 times $I_{\rm SD}$ for collapse of the QHR in butterfly-type Hall bars. These results show that the electronic structure in the Jaenneret-type Hall bar is not inhomogeneous like butterfly-type Hall bars discussed by Kawaji, Iizuka, Kuga and Okamoto.[110]

It has been known that the conduction due to electrons in the extended states thermally excited from localized states shows the temperature dependence of the resistivity given as

$$\rho_{xx}(T) = \rho_1 \exp(E_{\rm A}/k_{\rm B}T). \qquad [37]$$

Here, the variable range hopping is ignored as the temperature is not low enough. The activation energy depends on the Hall electric field $F_{\rm H}$ as

$$E_A = E_{A0} - ae\ell_B F_{\rm H} \qquad [38]$$

where $E_{\rm A0} = \hbar\omega_c/2$ and $\ell_B = \sqrt{(\hbar/eB)}$.[113)–115)] Numerical factor a depends on samples such as $a = 25$ in the $i = 4$ plateau,[113)] $a = 9$ in the $i = 2$ plateau[114)] and $a = 38 \pm 8$ in the $i = 4$ plateau.[115)] Figure 51 shows Shimada *et al.*'s experimental results[115)] where the activation energy $E_{\rm A}$ is normalized by $\hbar\omega_{\rm c}/2$ and the Hall electric field $F_{\rm H}$ is normalized by $(\hbar\omega_{\rm c}/2el_{\rm B})$.

$I_{\rm SD}$ dependence of ρ_{xx} in Fig. 50 can be explained for $I_{\rm SD} < 70\,\mu$A by Eq. [37] and [38] by using $a = 16.5$. Another effect of high Hall electric field may appear in electron heating.[112)]

Exact quantization of $R_{\rm H}(i)$ is expected in case of no dissipation, i.e., $\rho_{xx} = 0$. Finite dissipation is expected to produce deviation of $R_{\rm H}$ from the quantized value $R_{\rm H}(i)$, $\Delta R_{\rm H} = R_{\rm H} - R_{\rm H}(i)$, which is expected to be given by

$$|\Delta R_{\rm H}/R_{\rm H}(i)| \sim (\rho_{xx}/\rho_{xy})^2 \qquad [39]$$

from conductivity tensors and resistivity tensors.[116)] However, an experimental relation was derived as

$$\Delta R_{\rm H}/R_{\rm H}(i) = -s\rho_{xx}/R_{\rm H}(i) \qquad [40]$$

where s is given as $s \leq 0.15$,[76)] $s = 0.048$[117)] for Si-MOSFETs and s ranges from 0.507 to 0.015 in GaAs/AlGaAs heterostructures.[118)] However, the experimentally derived relation given by Eq. [40] has not been explained by basic electronic processes. In order to confirm the validity of the relation $R_{\rm K} = h/e^2$, we have to use a Hall device that shows the relation given by Eq. [39].

Figure 52 shows comparison of experimental

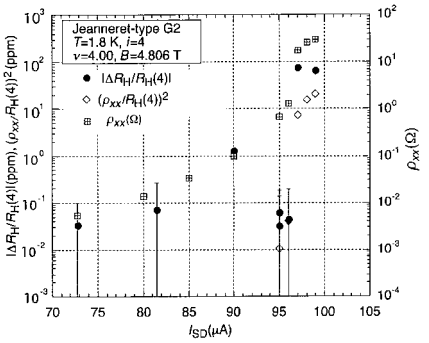

Fig. 52. Changes in absolute value of $\Delta R_{\rm H}/R_{\rm H}(4)$, $(\rho_{xx}/R_{\rm H}(4))^2$ and ρ_{xx} in logarithmic scales at a magnetic field at the center of the $i = 4$ Hall plateau ($\nu = 4$).[112]

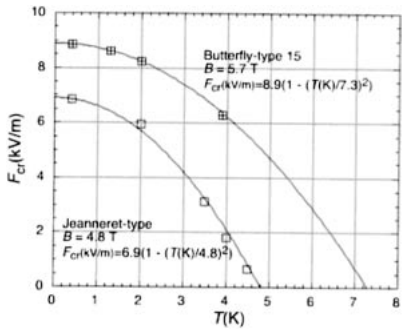

Fig. 53. Temperature dependence of critical Hall electric field $F_{\rm cr}$ for collapse of QHR. Each $F_{\rm cr}(T)$ cuve in this figure can be taken as the threshold curve that separates the QHE state from the non-QHE state in a $F - T$ plane.[119]

results of $|\Delta R_{\rm H}/R_{\rm H}(4)|$ and $(\rho_{xx}/R_{\rm H})^2$ plotted in a logarithmic scale. In Fig. 52, results calculated by Eq. [39] are about one tenth of experimental results of $\Delta R_{\rm H}/R_{\rm H}(4)$ in a region of $I_{\rm SD}$ higher than the breakdown current. They pointed out that ρ_{xx} used for calculation of $(\rho_{xx}/R_{\rm H}(4))^2$ is measured not in the region between opposite Hall probes but in the channel along $I_{\rm SD}$. When we take into account the fact that the Hall electric field $F_{\rm H}$ in the part for $R_{\rm H}$ measurement is lower than that in the part for ρ_{xx} measurement, agreement between $|\Delta R_{\rm H}/R_{\rm H}(4)|$ and $(\rho_{xx}/R_{\rm H})^2$ would be worse than that shown in Fig. 52. Further experimental studies using Hall bars having better electrode structures are needed.

Tanaka, Kawashima, Iizuka, Fukuda and Kawaji measured temperature dependence of critical current for the collapse of QHR in the butterfly-type and the Jeanneret-type Hall bars.[119] As it is known that the Hall electric field causes the QHR collapse,[109] the variations of the critical Hall electric field for the collapse $F_{\rm cr} = R_{\rm H}(4)I_{\rm cr}(T)/w$ with temperature T derived from the $I_{\rm cr}(T)$ in two samples are shown in Fig. 53. Each curve in this figure can be taken as the threshold curve that separates the QHE state on the lower left side of the figure from the non-QHE state on the upper right side in a $F - T$ plane.

The variation of $F_{\rm cr}(T)$ with temperature as shown in Fig. 53 is described by

$$F_{\rm cr}(T) = F_{\rm cr}(0)(1 - (T/T_{\rm cr})^2) \qquad [41]$$

as shown by each solid curve. The critical Hall electric field at absolute zero $F_{\rm cr}(0)$ and the critical temperature $T_{\rm cr}$ shown in Fig. 53 are summarized in Table 3. $F_{\rm cr}(0)$ in two Hall bars in Table 3 are proportional to $B^{3/2}$.

Table 3. Critical Hall electric field for collapse of QHR at zero temperature $F_{\rm cr}(0)$, critical temperature $T_{\rm cr}$ for $F_{\rm cr} = 0$ and Landau level splitting $\hbar\omega_{\rm c}$ in two samples in Fig. 53.[119]

Sample	B (T)	$F_{\rm cr}(0)$ (kV/m)	$T_{\rm cr}$ (K)	$\hbar\omega_{\rm c}$ (K)
Butterfly 15	5.7	8.9	7.3	112
Jeanneret 100	4.8	6.9	4.8	95

Tanaka *et al.*[119] discussed their experimental results on the basis of the electron localization picture of the QHE. They concluded that the temperature dependence of the critical Hall electric field for the collapse of QHR measured in two types of Hall bars can be explained using a model in which an inter-Landau level electron tunneling gives rise to the collapse of QHR with temperature dependence arising from the Fermi distribution function. Further experimental and theoretical studies of the collapse of QHR are necessary for a deeper understanding of the QHE.

8. Concluding remarks

(1) A two-dimensional semiconductor was created on a p-type Si surface by adsorption of Cs atoms.

(2) Understanding of the weak localization effect was established in two-dimensional systems in the temperature dependence of the conductivity and the negative magnetoresistance in n-channel inversion layers of Si and GaAs/$Al_{0.7}Ga_{0.3}As$ heterostructures.

(3) Understanding of the metal-insulator tran-

sition in two-dimensional systems was improved in Si-MOSFETs.

(4) Understanding of the Anderson localization in Landau levels in two-dimensional systems was improved including the electron-hole symmetry, the quantum Hall effect, the correlation between σ_{xx} and σ_{xy} and temperature dependence of localization. In these studies, our successful results of measurement of the Hall conductivity made the most important contribution to understanding of the phenomena.

(5) High precision measurements of the quantized Hall resistances in collaboration with members in NML (CSIRO) and ETL made contribution to understanding physics of the quantum Hall effect.

(6) Measurements of activation energies of the 1/3 and the 2/3 fractional quantum Hall effect for a lot of $GaAs/Al_{0.7}Ga_{0.3}As$ heterostructure samples left us some difficulties in understanding the phenpmenon in comparison with theoretical studies.

(7) Fundamental property of the breakdown of the quantum Hall effect was established by introducing butterfly-type Hall bars into the experimental study of the phenomenon. Our experience with the high precision measurements of the quantized Hall resistances made clear the phenomenon of the collapse of the quantized Hall resistance. Further studies of this phenomenon are expected to improve the understanding of the quantum Hall effect.

Acknowledgements

The author expresses his gratitude to Y. Kawaguchi, J. Wakabayashi, T. Okamoto, H. Kawashima and other members of his group in Gakushuin University. The author expresses his gratitude to G. Small and B. Ricketts at NML (CSIRO), C. Yamanouchi, K. Yoshihiro, J. Kinoshita and K. Inagaki at ETL for their help on the high precision measurements of QHR. The author expresses his gratitude to A. Yagi for Si-MOSFETs. The author also expresses his gratitude to T. Ando and A. Kawabata for their advice.

References

1) Bardeen, J. and Brattain, W.H. (1948) The transistor, a semiconductor triode. Phys. Rev. **74**, 230–231.
2) Many, A., Goldstein, Y. and Grover, N.B. (1965) Semiconductor Surfaces. North-Holland Publishing Co., Amsterdam.
3) Wilson, A.H. (1965) Theory of Metals. Cambridge University Press, Cambridge.
4) Schrieffer, J.R. (1955) Effective carrier mobility in surface-space charge layers. Phys. Rev. **97**, 641–646.
5) Kobayashi, A., Oda, Z., Kawaji, S., Arata, H. and Sugiyama, K. (1960) Impurity conduction of cleaned germanium surfaces at low temperatures. J. Phys. Chem. Solids **14**, 37–42.
6) Handler, P. and Eisenhour, S. (1964) Transport properties of light and heavy holes in the space charge region of a clean and water covered (111) germanium surface. Surf. Sci. **2**, 64–74.
7) Greene, R.F. (1964) Surface transport. Surf. Sci. **2**, 101–113.
8) Fowler, A.B., Fang, F.F., Howard, W.E. and Stiles, P.J. (1966) Oscillatory magneto-conductance in silicon surfaces. Proc. Int. Conf. Phys. Semicond. Kyoto. J. Phys. Soc. Jpn. **21**, 331–335; Fowler, A.B., Fang, F.F., Howard, W.E. and Stiles, P.J. (1966) Magneto-oscillatory conductance in silicon surfaces. Phys. Rev. Lett. **16**, 901–903.
9) Kawaji, S. and Kawaguchi, Y. (1966) Galvanomagnetic properties of surface layers in indium arsenide. Proc. Int. Conf. Phys. Semicond. Kyoto. J. Phys. Soc. Jpn. **21**, 336–340.
10) Conwell, E.M. and Weisskopf, V.F. (1950) Theory of impurity scattering in semiconductors. Phys. Rev. **77**, 388–390.
11) Stern, F. and Howard, W.E. (1967) Properties of semiconductor surface inversion layers in the electric quantum limit. Phys. Rev. **163**, 816–835.
12) Ando, T., Fowler, A.B. and Stern, F. (1982) Electronic properties of two-dimensional systems. Rev. Mod. Phys. **54**, 437–672.
13) Kawaji, S. (1994) Quantum transport in semiconductor surface and interface channels. Surf. Sci. **299/300**, 563–586.
14) Mimura, T., Hiyamizu, S., Fujii, T. and Nanbu, K. (1980) A new field-effect transistor with selectively doped $GaAs/Al_xGa_{1-x}As$ heterojunctions. Jpn. J. Appl. Phys. **19**, L225–L227.
15) Mimura, T., Hiyamizu, S., Joshin, K. and Hikosaka, K. (1981) Enhance-mode high electron mobility transistors for logic applications. Jpn. J. Appl. Phys. **20**, L317–L319.
16) Kawaguchi, Y. (1976) Electrical conduction in silicon surface inversion layers by adsorption of Cs atoms. Thesis, Gakushuin University (March, 1976) (in Japanese).
17) Kawaguchi, Y. and Kawaji, S. (1976) Impurity band conduction in cesium adsorbed n-channel Si inversion layers. Surf. Sci. **58**, 33–41.
18) Pearson, G.L. and Bardeen, J. (1949) Electrical properties of pure silicon and silicon alloys containing boron and phosphorus. Phys. Rev. **75**, 865–883.
19) Kawaguchi, Y., Kitahara, H. and Kawaji, S.

(1978) Negative magnetoresistance in a two dimensional impurity band in cesiated p-Si (111) surface inversion layers. Surf. Sci. **73**, 520–527.

20) Kawaguchi, Y., Kitahara, H. and Kawaji, S. (1978) Angular dependent negative magnetoresistance in Si-MOS(111) inversion layers. Solid State Comm. **26**, 701–703.
21) Thouless, D.J. (1977) Maximum metallic resistance in thin wires. Phys. Rev. Lett. **39**, 1167–1169.
22) Abrahams, E., Anderson, P.W., Licciardello, D.C. and Ramakrishnan, T.V. (1979) Scaling theory of localization: Absence of quantum diffusion in two dimensions. Phys. Rev. Lett. **42**, 673–676.
23) Anderson, P.W., Abrahams, E. and Ramakrishnan, T.V. (1979) Possible explanation of nonlinear conductivity in thin-film metal wires. Phys. Rev. Lett. **43**, 718–720.
24) Gorkov, L.P., Larkin, A.I. and Khmel'nitskii, D.E. (1979) Particle conductivity in a two-dimensional random potential. Pisma Zh. ETF. **30**, 248–252 [JETP Lett. **30**, 228–232].
25) Hikami, S., Larkin, A.I. and Nagaoka, Y. (1980) Spin-orbit interaction and magnetoresistance in the two dimensional random system. Prog. Theor. Phys. **63**, 707–710.
26) Fukuyama, H. (1982) Theory of weakly localized regime of the Anderson localization in two dimensions. Surf. Sci. **113**, 489–504.
27) Nagaoka, Y. and Fukuyama, H. (eds.) (1982) Anderson Localization. Springer-Verlag, Berlin-New York.
28) Kmel'nitskii, D.E. (1984) Localization and coherent scattering of electrons. Physica **126B**, 235–241.
29) Uemura, Y. (1974) Landau levels and electronic properties of semiconductor interface. Proc. Int. Conf. Solid Surfaces. Jpn. J. Appl. Phys. Suppl. **2**, Pt. 2, 17–24.
30) Ohkawa, F.J. and Uemura, Y. (1977) Theory of valley splitting in an n-channel (100) inversion layer of Si. I. Formulation by extended zone effective mass theory. J. Phys. Soc. Jpn. **43**, 907–916; Ohkawa, F.J. and Uemura, Y. (1977) Theory of valley splitting in an N-channel(100) inversion layer of Si II. Electric break through. J. Phys. Soc. Jpn. **43**, 917–924; Ohkawa, F. J. and Uemura, Y. (1977) Theory of valley splitting in an N-channel(100) inversion layer of Si III. Enhancement of splittings by many-body effects. J. Phys. Soc. Jpn. **43**, 925–932.
31) Bishop, D.J., Tsui, D.C. and Dynes, R.C. (1980) Nonmetallic comduction in electron inversion layers at low temperatures. Phys. Rev. Lett. **44**, 1153–1156.
32) Kawaguchi, Y. and Kawaji, S. (1980) Negative magnetoresistance in silicon (100) MOS inversion layers. J. Phys. Soc. Jpn. **48**, 699–700.
33) Kawaguchi, Y. and Kawaji, S. (1981) Negative magnetoresistance in a two-dimensional random system of Si-MOS inversion layers. Proc. 15th Int. Cof. Physics of Semicond. Kyoto, 1980. J. Phys. Soc. Jpn. **49** (Suppl. A), 983–986.
34) Kawaguchi, Y. and Kawaji, S. (1982) A study of electron mobility and electron-phonon interaction in Si MOSFETs by negative magnetoresistance experiments. Jpn. J. Appl. Phys. **21**, part 2, L709–L711.
35) Ezawa, H., Kawaji, S. and Nakamura, K. (1974) Surfons and the electron mobility in silicon inversion layers. Jpn. J. Appl. Phys. **13**, 126–155.
36) Shinba, Y., Nakamura, K., Fukuchi, M. and Sakata, M. (1982) Hot electrons in Si(100) inversion layers at low lattice temperatures. J. Phys. Soc. Jpn. **51**, 157–163.
37) Poole, D.A., Pepper, M. and Glew, D.A. (1981) The observation of localization and interaction effects in the two-dimensional electron gas of a GaAs-$Al_xGa_{1-x}As$ heterostructures. J. Phys. **C14**, L995–L1005.
38) Lin, B.J., Paalanen, M.A., Gossard, A.C. and Tsui, D.C. (1984) Weak localization of two-dimensional electrons in GaAs-$Al_xGa_{1-x}As$ heterostructures. Phys. Rev. **B29**, 927–934.
39) Nambu, T., Kawaji, S., Kuboki, K., Kawaguchi, Y., Yoshino, J. and Sakaki, H. (1984) Negative magnetoresistance and inelastic scattering time in two-dimensional electron systems in GaAs/$Al_xGa_{1-x}As$ heterojunction interfaces. J. Phys. Soc. Jpn. **53**, 682–686.
40) Fukuyama, H. and Abrahams, E. (1983) Inelastic scattering time in two-dimensional disordered metals. Phys. Rev. **B27**, 5976–5980.
41) Kawabata, A. (1984) On the field dependence of magnetoresistance in two-dimensional systems. J. Phys. Soc. Jpn. **53**, 3540–3544.
42) Kawabata, A. (1980) Theory of negative magnetoresistance I. Application to heavily doped semiconductors. J. Phys. Soc. Jpn. **49**, 628–637.
43) Kawaji, S. (1985) Experiments on localization in semiconductor two-dimensional systems. Progr. Theor. Phys. Suppl. **84**, 178–214.
44) Kawaji, S., Kuboki, K., Shigeno, H., Nambu, T., Wakabayashi, J., Yoshino, J. and Sakaki, H. (1985) Inelastic scattering and spin-orbit scattering in 2D systems of GaAs/AlGaAs heterostructures. *In* Proc. 17th Int. Conf. on Physics of Semicond. (eds. Chadi, J.D. and Harrison, W.A.). Springer-Verlag, Berlin-New York, pp. 413–416.
45) Kawaji, S. and Kawaguchi, Y. (1984) Negative magnetoresistance and inelastic scattering time in Si-MOS inversion layers. J. Phys. Soc. Jpn. **53**, 2868–2871.
46) Kawaji, S. (1986) Weak localization and negative magnetoresistance in semiconductor two-dimensional systems. Surf. Sci. **170**, 682–700.
47) Okamoto, T., Hosoya, K., Kawaji, S. and Yagi, A. (1999) Spin degree of freedom in a two-dimensional electron liquid. Phys. Rev. Lett. **82**, 3875–3878.
48) Kravchenko, S.V., Kravchenko, G.V., Furneaux,

J.E, Pudalov, V.M. and D'Iorio, M. (1994) Possible metal-insulator transition at $B = 0$ in two dimensions. Phys. Rev. **B50**, 8039–8042.
49) Tutuc, E., De Portere, E.P., Papadakis, S.J. and Shayegan, M. (2001) In-plane magnetic field-induced spin polarization and transition to insulating behavior in two-dimensional Hole system. Phys. Rev. Lett. **86**, 2858–2861.
50) Okamoto, T., Ooya, M., Hosoya, K. and Kawaji, S. (2004) Spin polarization and metallic behavior in a silicon two-dimensional system. Phys. Rev. **B69**, 041202.
51) Kawaji, S. and Wakabayashi, J. (1976) Quantum galvanomagnetic properties of n-type inversion layers on Si(100) MOSFET. Surf. Sci. **58**, 238–245.
52) Kawaji, S. and Wakabayashi, J. (1977) Temperature dependence of the magnetoconductivity in the ground Landau level in silicon inversion layers. Solid State Comm. **22**, 87–91.
53) Ando, T., Matsumoto, Y. and Uemura, Y. (1975) Theory of Hall effect in a two-dimensional electron system. J. Phys. Soc. Jpn. **39**, 279–288.
54) Ando, T. (1974) Private communications.
55) Igarashi, T., Wakabayashi, J. and Kawaji, S. (1975) Hall effect in silicon inversion layers under strong magnetic fields. J. Phys. Soc. Jpn. **38**, 1549.
56) Kawaji, S., Igarashi, T. and Wakabayashi, J. (1975) Quantum galvanomagnetic effect in n-channel silicon inversion layers under strong magnetic fields. Prog. Theor. Phys. Suppl. **57**, 176–186.
57) Wick, R.F. (1954) Solution of the field problem of the germanium gyrator. J. Appl. Phys. **25**, 741–756.
58) Ando, T. and Uemura, Y. (1974) Theory of quantum transport in a two-dimensional electron system under magnetic field. I. Characteristics of level broadening and transport under magnetic fields. J. Phys. Soc. Jpn. **36**, 959–967.
59) Wakabayashi, J. and Kawaji, S. (1978) Hall effect in silicon MOS inversion layers under strong magnetic fields. J. Phys. Soc. Jpn. **44**, 1839–1849.
60) Wakabayashi, J. and Kawaji, S. (1980) Hall conductivity in n-type silicon inversion layers under strong magnetic fields. Surf. Sci. **98**, 299–307.
61) Kawaji, S. and Wakabayashi, J. (1981) Temperature dependence of transverse and Hall conductivities of silicon MOS inversion layers under strong magnetic fields. Proc. Oji Int. Symposium, Hakone, 1980, Physics in High Magnetic Fields (eds. Chikazumi, S. and Miura, N.). Springer, Berlin, pp. 284–287.
62) Kawaji, S. (1984) Quantum Hall effect. Proc. Int. Symp. Foundation of Quantum Mechanics, Tokyo, 1983. Phys. Soc. Jpn. 1984, pp. 327–338.
63) Levine, H.S., Libby, B. and Pruisken, A.M.M. (1983) Electron delocalization by a magnetic field in two dimensions. Phys. Rev. Lett. **51**, 1915–1918.
64) Ando, T. (1983) Electron localization in a two-dimensional system in strong magnetic fields. I. Case of short range scatterers. J. Phys. Soc. Jpn. **52**, 1740–1749; Ando, T. (1984) Electron localization in a two-dimensional system in strong magnetic fields. II. Long range scatterers and response function. J. Phys. Soc. Jpn. **53**, 3101–3111; Ando, T. (1984) Electron localization in a two-dimensional system in strong magnetic fields. III. Impurity concentration dependence and level mixing effects. J. Phys. Soc. Jpn. **53**, 3126–3135.
65) Aoki, H. and Ando, T. (1984) Critical localization in two-dimensional Landau quantization. Phys. Rev. Lett. **54**, 831–834.
66) Ando, T. and Aoki, H. (1985) Finite-size scaling study of localization in Landau levels. J. Phys. Soc. Jpn. **54**, 2238–2249.
67) Aoki, H. and Ando, T. (1986) Critical localization and low-temperature transport in two-dimensional Landau quantization. Surf. Sci. **170**, 249–255.
68) Yamane, M., Wakabayashi, J. and Kawaji, S. (1989) Experimental correlation between diagonal and Hall conductivities of silicon MOS inversion layers in strong magnetic fields. J. Phys. Soc. Jpn. **58**, 1899–1902.
69) Kawaji, S., Wakabayashi, J. and Moriyama, J. (1981) Analysis of temperature dependent Hall conductivity in silicon inversion layers in strong magnetic fields by a mobility edge model. J. Phys. Soc. Jpn. **50**, 3839–3840.
70) Moriyama, J. and Kawaji, S. (1983) Temperature dependence of effective mobility edge and inelastic scattering time in silicon MOS inversion layers in strong magnetic fields. Solid State Comm. **45**, 511–513.
71) Wakabayashi, J., Yamane, M. and Kawaji, S. (1989) Experiments on the critical exponent of localization in Landau subbands with the Landau quantum number 0 and 1 in Si-MOS inversion layers. J. Phys. Soc. Jpn. **58**, 1903–1905.
72) von Klitzing, K., Dorda, G. and Pepper, M. (1980) New method for high accuracy determination of the fine-structure constant based on quantized Hall resistance. Phys. Rev. Lett. **45**, 494–497.
73) Yamanouchi, C., Yoshihiro, K., Kinoshita, J., Inagaki, K., Moriyama, J., Baba, S., Kawaji, S., Murakami, K., Igarashi, T., Endo, T. *et al.* (1984) Hall effect in silicon MOS inversion layers — For h/e^2 determination. Precision Measurements and Fundamental Constants II (eds. Taylor, B.N. and Phillips, W.D.). NBS USA Spec. Publ. **617** (1984), pp. 529–534.
74) Yoshihiro, K., Kinoshita, J., Inagaki, K., Yamanouchi, C., Moriyama, J. and Kawaji, S. (1982) Quantized Hall resistivity in Si-MOSFETs measured at liq. ^{3}He temperature. J. Phys. Soc. Jpn. **51**, 5–6.
75) Kinoshita, J., Inagaki, K., Yamanouchi, C.,

Yoshihiro, K., Moriyama, J. and Kawaji, S. (1983) Determination of $h/4e^2$—A preliminary measurement based on the quantized Hall effect of Si-MOSFETs. Report submitted to 16^e Session, Comité Consultatif d'Électricite (March 1983).

76) Yoshihiro, K., Kinoshita, J., Inagaki, K., Yamanouchi, C., Endo, T., Murayama, Y., Koyanagi, M., Yagi, A., Wakabayashi, J. and Kawaji, S. (1986) Quantum Hall effect in silicon metal-oxide-semiconductor inversion layers: experimental conditions for determination of h/e^2. Phys. Rev. **B33**, 6874–6896.

77) Kinoshita, J., Inagaki, K., Yamanouchi, C., Yoshihiro, K., Kawaji, S., Nagashima, N., Kikuchi, N. and Wakabayashi, J. (1989) Self-balancing resistance ratio bridge using a cryogenic current comparator. IEEE Trans. Instrum. Meas. **38**, 290–292.

78) Small, G.W. (1983) Comparison of quantized Hall resistance with a 1-Ω resistor. IEEE Trans. Instrum. Meas. **IM-32**, 446–447.

79) Small, G.W. (1987) Twenty years of SI ohm determination at NML. IEEE Trans. Instrum. Meas. **IM-36**, 190–195.

80) Kawaji, S., Nagashima, N., Kikuchi, N., Wakabayashi, J., Ricketts, B., Yoshijiro, K., Kinoshita, J., Inagaki, K. and Yamanouchi, C. (1989) Quantized Hall resistance measurements. IEEE Trans. Instrum. Meas. **IM-38**, 270–275.

81) Taylor, B.N. and Witt, T.J. (1989) New international resistance standards based on the Josephson and quantum Hall effects. Metrologia **26**, 47–62.

82) Nagashima, N., Date, M., Wakabayashi, J., Kawaji, S., Yoshihiro, K., Kinoshita, K., Inagaki, K. and Yamanouchi, C. (1994) Comparison of quantized Hall resistances $R_{\rm H}(2)$ and $R_{\rm H}(4)$ of a GaAs/AlGaAs heterostructure device. IEEE Trans. Instrum. Meas. **43**, 521–525.

83) Nagata, M. (1993) High precision measurements of quantized Hall resistances. Master Thesis, Gakushuin University (March 1993) (in Japanese).

84) Hayashi, K. (1995) High precision measurements of quantized Hall resistances. Master Thesis, Gakushuin University (January 1995) (in Japanese).

85) Tsui, D.C., Stormer, H.L. and Gossard, A.C. (1982) Two-dimensional magnetotransport in extreme quantum limit. Phys. Rev. Lett. **48**, 1559–1562.

86) Tsui, D.C., Stormer, H.L., Hwang, J.C.M., Brooks, J.S. and Naughton, M.J. (1983) Observation of a fractional quantum number. Phys. Rev. **B28**, 2274–2275.

87) Yoshioka, D., Halperin, B.I. and Lee, P.A. (1983) Ground state of two-dimensional electrons in strong magnetic fields and 1/3 quantized Hall effect. Phys. Rev. Lett. **50**, 1219–1222.

88) Laughlin, R.B. (1983) Anomalous quamtum Hall effect: An incompressible quantum fluid with fractionally charged excitations. Phys. Rev. Lett. **50**, 1395–1398.

89) Tau, R. and Thouless, D.J. (1983) Fractional quantization of Hall conductance. Phys. Rev. **B28**, 1142–1144.

90) Laughlin, R.B. (1984) Primitive and composite ground states in the fractional quantum Hall effect. Surf. Sci. **142**, 163–172.

91) Chacraborty, T. (1985) Elementary excitations in the fractional quantum Hall effect. Phys. Rev. **B31**, 4026–4028.

92) Haldane, F.D.M and Rezayi, E.H. (1985) Finite-size studies of the incompressible state of the fractionally quantized Hall effect and its excitations. Phys. Rev. Lett. **54**, 237–240.

93) Yoshioka, D. (1985) Theory of the fractional quantum Hall effect. Progr. Theor. Phys. Suppl. **84**, 97–119.

94) Chang, A.M., Paalanen, M.A., Tsui, D.C., Stormer, H.L. and Hwang, J.C.M. (1983) Fractional quantum Hall effect at low temperatures. Phys. Rev. **B28**, 6133–6136.

95) Kawaji, S., Wakabayashi, J., Yoshino, J. and Sakaki, H. (1984) Activation energies of the 1/3 and 2/3 fractional quantum Hall effect in $GaAs/Al_xGa_{1-x}As$ heterostructures. J. Phys. Soc. Jpn. **53**, 1915–1918.

96) Wakabayashi, J., Kawaji, S., Yoshino, J. and Sakaki, H. (1986) Activation energies of the fractional quantum Hall effect in GaAs/AlGaAs heterostructures. J. Phys. Soc. Jpn. **55**, 1319–1326.

97) Wakabayashi, J., Kawaji, S., Yoshino, J. and Sakaki, H. (1986) Activation energies of the 1/3 and 2/3 fractional quantum Hall effect. Surf. Sci. **170**, 136–140.

98) Wakabayashi, J., Sudou, S., Kawaji, S., Hirakawa, K. and Sakaki, H. (1987) Second activation energy in the fractional quantum Hall effect. J. Phys. Soc. Jpn. **56**, 3005–3008.

99) Wakabayashi, J., Sudou, S., Kawaji, S., Hirakawa, K. and Sakaki, H. (1987) Activation energies of the 2/3 fractional quantum Hall effect in a GaAs/AlGaAs heterostructure with a backgside gate. Proc. 18th Int. Conf. Semicond. (ed. Engstrom, O.). World Scientific. Singapore, pp. 425–428.

100) Wakabayashi, J. (1987) Activation energies of the fractional quantum Hall effect. Proc. Int. Conf. of High Magnetic Fields in Semiconductor Physics (ed. Landwehr, G.). Springer-Verlag, Berlin, pp. 156–165.

101) Wakabayashi, J., Sudou, S., Kawaji, S., Hirakawa, K. and Sakaki, H. (1988) Effects of the gate bias on the activation energies of the fractional quantum Hall effect. Surf. Sci. **196**, 236–241.

102) Boebinger, G.S., Chang, A.M., Stormer, H.L. and Tsui, D.C. (1985) Magnetic field dependence of activation energies of the fractional quantum Hall effect. Phys. Rev. Lett. **55**, 1606–1609.

103) Ebert, G., von Klitzing, K., Ploog, K. and

Weiman, G. (1983) Two-dimensional magneto-quantum transport on GaAs-$Al_xGa_{1-x}As$ heterostructure under non-ohmic conditions. J. Phys. C. Solid State Phys. **16**, 5441–5448.
104) Cage, M.E., Dziuba, R.F., Field, B.F., Williams, E.R., Girvin, S.M., Gossard, A.C. and Tsui, D.C. (1983) Dissipation and dynamic nonlinear behavior in the quantum Hall regime. Phys. Rev. Lett. **51**, 1374–1377.
105) Kawaji, S., Hirakawa, K., Nagata, N., Okamoto, T., Fukase, T. and Goto, T. (1994) Breakdown of the quantum Hall effect in GaAs/AlGaAs heterostructures due to current. J. Phys. Soc. Jpn. **63**, 2303–2313.
106) Okuno, T., Kawaji, S., Ohrui, S., Okamoto, T., Kurata, Y. and Sakai, J. (1995) Electron concentration and mobility dependence of breakdown of the quantum Hall effect. J. Phys. Soc. Jpn. **64**, 1881–1884.
107) Kawaji, S. (1996) Breakdown of the integer quantum Hall effect at high currents in GaAs/AlGaAs heterostructures. Semicond. Sci. Technol. **11**, 1546–1551.
108) Eaves, L. and Sheard, F.W. (1986) Size-dependent quantized breakdown of the dissipationless quantum Hall effect in narrow channels. Semicond. Sci. Technol. **1**, 346–349.
109) Kawaji, S., Suzuki, J., Shimada, T., Iizuka, H., Kuga, T. and Okamoto, T. (1998) Collapse of quantized Hall resistance and breakdown of IQHE in GaAs/AlGaAs heteostructures. J. Phys. Soc. Jpn. **67**, 1110–1113.
110) Kawaji, S., Iizuka, H., Kuga, T. and Okamoto, T. (1998) Collapse of quantized Hall resistance at high electric fields. Physica B **256–258**, 56–57.
111) Jeanneret, B., Jeckelmann, B., Bühlmann, H.J., Houdé, R. and Ilegems, M. (1995) Influence of the device-width on the accuracy of quantization in the integer quantum Hall effect. IEEE Trans. Instrum. Meas. **44**, 254–257.
112) Kawashima, H., Tanaka, H. and Kawaji, S. (2005) Collapse of the quantized Hall resistance and role of the diagonal resistivity in the quantum Hall effect. J. Phys. Soc. Jpn. **74**, 2791–2796.
113) Komiyama, S., Takamasu, T., Hiyamizu, S. and Sasa, S. (1985) Breakdown of the quantum Hall effect due to electron heating. Solid State Commun. **54**, 479–484.
114) Boisen, A., Boggild, P., Kristensen, A. and Lindelof, P.E. (1994) Nonlinear current-voltage characteristics at quantum Hall resistance minima. Phys. Rev. **B50**, 1957–1960.
115) Shimada, T., Okamoto, T. and Kawaji, S. (1998) Hall electric field-dependent broadening of extended state bands in Landau levels and breakdown of the quantum Hall effect. Physica B **249–251**, 107–110.
116) Laughlin, R.B. (1982) Impurities and edges in the quantum Hall effect. Surf. Sci. **113**, 22–26.
117) Hartland, A., Jones, K., Williams, J.M., Gallagher, B.L. and Galloway, T. (1991) Direct comparison of the quantized Hall resistance in gallium arsenide and silicon. Phys. Rev. Lett. **66**, 969–973.
118) Cage, M.E., Field, B.F., Dziuba, R.F., Girvin, S.M., Gossard, A.C. and Tsui, D.C. (1984) Temperature dependence of the quantum Hall resistance. Phys. Rev. **B30**, 2286–2288.
119) Tanaka, H., Kawashima, H., Iizuka, H., Fukuda, H. and Kawaji, S. (2006) Temperature dependence of collapse of quantized Hall resistance. J. Phys. Soc. Jpn. **75**, 014701.

(Received Mar. 24, 2008; accepted May 7, 2008)

Profile

Shinji Kawaji was born in 1932 in Hokkaido, Japan. He graduated from Hokkaido University, Faculty of Science, Department of Physics in 1953 and started his research carrier in experimental study on "Surface Potential and Adsorption of Gases on Semiconductors" in Professor Akio Kobayashi's laboratory in the Research Institute for Catalysis. After receiving Ph.D. degree in 1958 from Hokkaido University under the guidance of Professor Jiro Furuichi, he joined Gakushuin University, Faculty of Science, Department of Physics as a lecturer and opened his laboratory. In the meantime, he stayed at Professor H. C. Gatos's laboratory in Massachusetts Institute of Technology in Cambridge, USA, for about 2 years between the end of 1963 and the beginning of 1965 as a research associate and carried out measurements of electrical properties of III–V compound semiconductor surfaces. He presented a paper on electrical conduction of a two-dimensional electron system (2DES) in an InAs surface in the International Conference on Physics of Semiconductors held in Kyoto in 1966. It was one of two papers which opened the new field. He initiated experimental studies of weak localization effect in the 2DES in 1978 and discovered quantum Hall effect in 1980. He continued experimental researches on quantum transport phenomena in 2DES until his retirement in 2002. He served as the Regional Editor of the International Journal "Surface Science (Elsevier)" in Japan from 1981 to 1996. He was awarded the Nishina Memorial Award in 1984, the Toray Science and Technology Award in 1992, the Medal with Purple Ribbon in 1994 and the Japan Academy Prize in 2007.